

Design Report
FEEG6013 Group Design Project

25
VENAS
Veneer Assessment System

Project Summary:

The evaluation of wood veneers is a handcrafted industry where qualitative analysis of wood veneer is performed through human inspection. The knowledge of this assessment is non-transferable as it is experienced based. Adding to that, assessing wood veneers for the regions of stress concentrations is subjective to the person, which is not reliable. This project aims to address these issues through the utilisation of a data-driven approach. The Veneer Assessment System evaluates features of wood veneers that are causing high stress concentrations during the forming process through an automated system which provides the user with guidance on regions to avoid or strategically position before the veneer has undergone forming. As a result, the Veneer Assessment System provides a consistent detection accuracy of 63% in detecting sycamore wood veneer..

Group Members:

ID Number	Name
31486894	Ven Chung Khoo
31145914	Yee Jie Tan
30959276	Thomas Turner
31395104	Ong Ian Bo
32248946	Yann Heng Yap
30640345	Yuk Cheong Tang

Primary Supervisor: Dr. Richard Cook

Co-Supervisors: Dr. Meisam Jalalvand

Submitted on: 09/05/2024

Table of Contents

Table of Contents	2
1 Introduction	2
2 Aims and Objectives	3
3 Investigation	4
4 Hardware	7
5 Operating System	19
6 Electronics	19
7 Software	20
8 Prototyping & Concept Proofing	27
9 Summary	Error! Bookmark not defined.
10 Appendix A (Section 3: Investigation)	31
11 Appendix B (Section 4: Hardware)	32

Acknowledgement

We would like to express our gratitude to our supervisors, Richard Cook and Meisam Jalalvand for their guidance throughout the entirety of the project.

1 Introduction

1.1 Project Stakeholders

The evaluation of wood veneers for automobile interior design traditionally relies on visual inspection and subjective human judgement to identify regions prone to stress concentration during the forming process. This process involves forming the veneer onto an uneven surface through bending. However, this method of veneer assessment is prone to inconsistency, as it relies on individual experience and expertise, making the skill non-transferable to others.

It has been recognised that this approach has limitations, and therefore a request has been made by our primary stakeholder, a luxury automobile company, for the development of a data-driven method integrated with an automated system to assess veneers. The objective is to identify and avoid stress concentration points during the manufacturing process, particularly during bending. This has led to the conception of VENAS, a project aimed at developing a fully automated system capable of assessing wood veneers and identifying all potential stress concentration points using validated data-driven knowledge.

The additional stakeholders involved in the project are outlined in Table 1. Subsequently, a meeting was convened with the primary stakeholder to delve deeper into their requirements. The detailed requirements of the primary stakeholder were documented in Table 2. These key insights were then utilized to craft a comprehensive design brief, alongside design specifications, serving as fundamental guidelines throughout the design process.

Stakeholders	Description
Luxury Automotive Company	Primary client and beneficiary representing the luxury automotive industry's interests.
Operators	System end users responsible for system operation and regular interaction.
Car Owners	End users owning or using luxury vehicles with wood veneer components.
Environmental Agencies	External organizations focused on environmental preservation and sustainability, with an interest in wood veneer usage's ecological impact.
Supervisors	Overseers providing guidance and oversight.
Furniture Companies	Entities in the furniture sector using wood veneers as a primary material.
Regulatory Bodies	Government or industry organizations establishing standards and regulations for wood veneer products and manufacturing.
Health and Safety Authorities	Agencies ensuring worker and consumer safety in relevant industries.
Legal Advisors	Legal professionals advising on regulatory compliance, contracts, and intellectual property.

Table 1.1-1 List of Identified Stakeholders

1.2 Project Scope

Aspect	Description
Method of Analysis	The analysis method should be data-driven, relying on experimental evidence simulating stress conditions during the forming process.
Veneer Type	Focus primarily on sycamore wood veneer, with adaptability to address stress concentration in other veneer types of varying sizes.
Veneer Size	Largest veneer analyzed: 720mm x 125mm
Environment	System operates under factory atmospheric conditions.
Success Criteria and Expectations	Target minimum accuracy: 68%, equivalent to current human inspection accuracy.
Output Expectations	Output presented visually, offering clear and concise insights into veneer condition.

Table 1.2-1: Primary Stakeholder Requirements

2 Aims and Objectives

2.1 Design Brief

VENAS serves as a proof of concept for an integrated system-level assessment tool, reliably predicting stress concentration features on engineered wood veneer sheets based on grain pattern imaging. Its purpose is to guide cutting operations before forming processes, ensuring avoidance or strategic positioning of weak regions to minimize damage during contour form pressing. Aligned with primary stakeholder specifications, the project aims to achieve the following objectives:

Aim:

Develop and implement a data-driven system capable of accurately detecting stress concentration regions in veneer before forming, offering guidance to operators to mitigate damage during pressing by avoiding or strategically positioning these areas.

Objectives:

1. Identify and analyse features causing high stress concentrations in veneer during the forming process, providing comprehensive insights into their condition.
2. Develop a versatile system capable of assessing veneer sizes up to 720mm x 125mm or smaller.
3. Design a portable tool for convenient structural assessment use in various locations.
4. Attain a detection accuracy exceeding 68%, surpassing human inspection capabilities.

2.2 Team Structure

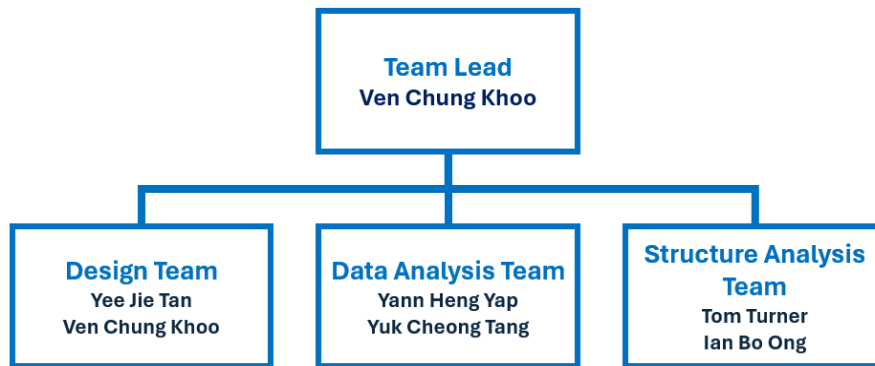


Figure 2.2-1 Team Structure Tree

The project's organizational structure comprises three specialized teams: the Design Team, responsible for hardware development; the Data Analysis Team, focused on software development; and the Structure Analysis Team, tasked with examining wood veneer properties. While each team has distinct responsibilities, collaborative interactions facilitate integration and comprehensive development across project stages.

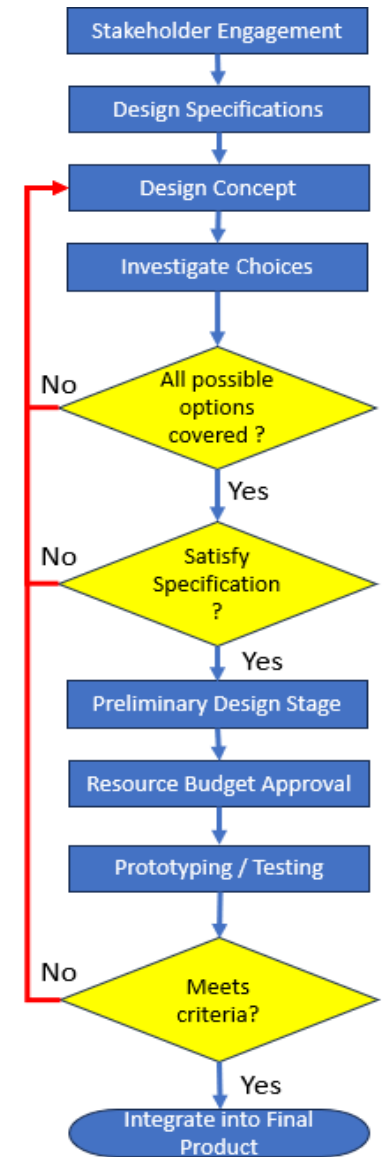
2.3 Target Design Specification

Two separate design specifications for two different products were created in accordance with the stakeholder requirements. This is due to the various requirements that were specified which outreaches the capabilities of the product. Below addresses the target specifications that the Photoimaging Gantry Setup and Cake Tier Apparatus should achieve, and the success criteria of these tools will be assessed off the specification as well as the aims and objectives.

The cake tier apparatus specification was created after the second stakeholder engagement, where their demands were focused on the portability of the apparatus, as well as it being suited for other types of wood veneer.

Photoimaging Gantry Setup		
Specifications		Target Parameter
Maximum Veneer Size		Accommodating veneer size of 720mm x 125mm
Environmental Considerations and Material Usage		Recyclable materials: 60% minimum of system components
Operating Conditions		35% humidity at 20-25°C (Atmospheric Conditions)
Assessment	Target Detection Rate	≥68%
	Autonomous Requirement	Scan entire veneer without omissions or repetitions
	Versatility	Ability to assess veneers of various sizes
User Considerations		Integration with computer system for data processing
Safety	Compliance with EN ISO12100:2010	
	Noise Levels: <70dB to prevent hearing damage[1]	

Table 2.3-1 Design Specification for Gantry Setup



Cake Tier Apparatus		
Specifications		Target Parameter
Portability		Weight: Below 1.4kg for ergonomic portability
Imitate Forming Process		Ability to simulate veneer forming process
Versatility		Compatibility with various types of veneer
Environmental Considerations and Material Usage		Recyclable materials: 60% minimum of apparatus
User Consideration		Ease of operation without specialised training
Varying Diameter		Samples should be able to be tested at varying diameters as different veneers will have a range of critical bending radii.

Table 2.3-2. Design Specification for Cake Tier Apparatus

3 Investigation

To meet the project objectives, thorough investigation of the veneer is imperative to identify stress concentrations or weak points. This information forms the cornerstone of the project, guiding all subsequent design processes, both hardware and software.

3.1 Initial Investigation

3.1.1 C-T

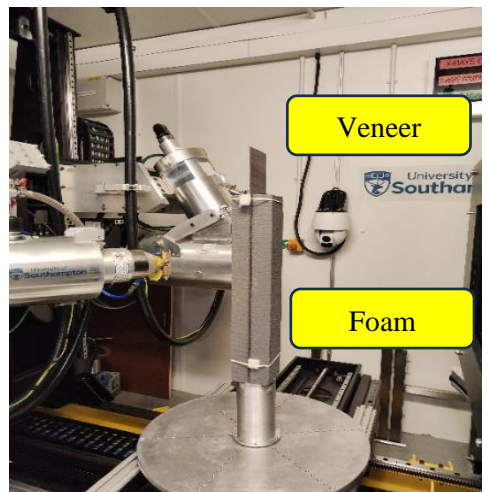


Figure 3.1.1 - 1: C-T Apparatus.

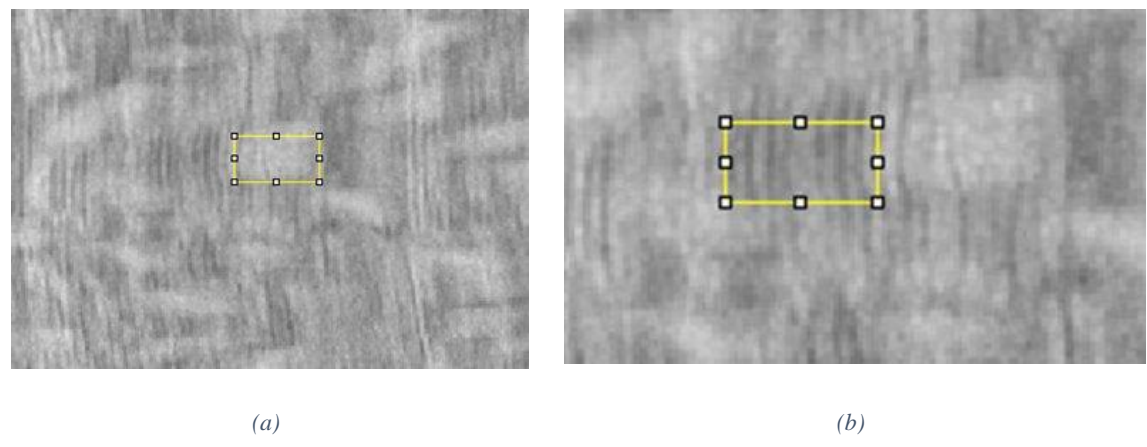


Figure 3.1.1 - 2: (a) Dark Patches. (b) Light Patches.

3.1.2 Microscope

Some features visible to the naked eye are directly related to the structural aspects of the wood. For example, the horizontal grain pattern in Figure 3.1.1 - 2(b) represents fibres that are not necessarily straight but wavy. Rays, depicted as vertical patches in the red circle within Figure 3.1.2 - 2(b), scatter across the veneer and are observable as "lighter speckle patterns." Interestingly, further investigation reveals that the speckle pattern appears either light or dark depending on the lighting direction and intensity.

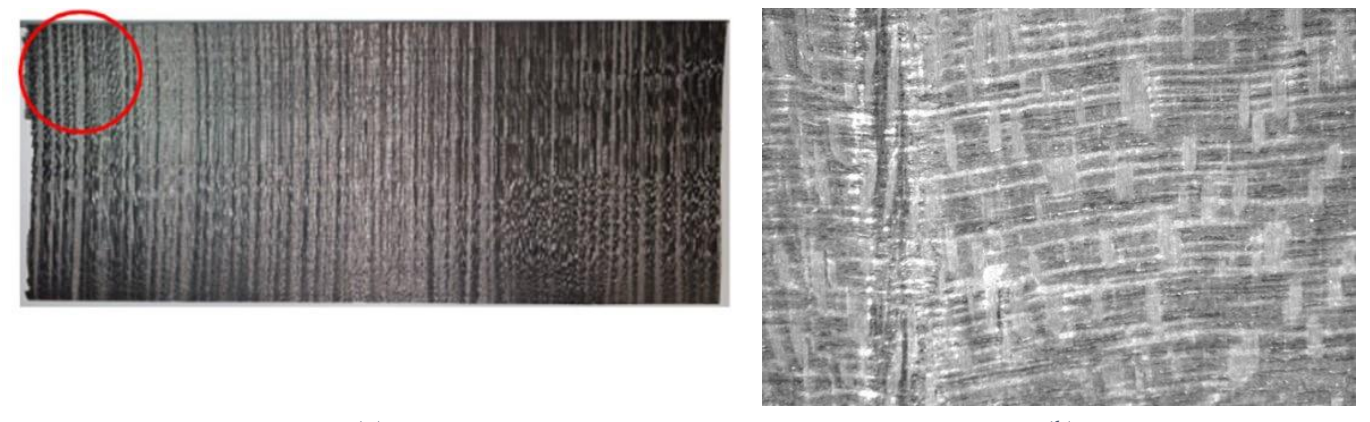


Figure 3.1.2 - 1: (a) The veneer piece put under microscope. (b) 2x Magnification of the area circled in red.
The pre-existing fracture regions of the veneer were examined under a microscope to identify common features associated with the fractures. It was discovered that all fractures investigated occurred around the presence of rays, indicating a high likelihood that the change in grain direction directly contributed to the fractures. Figure 3.1.2 - 2 below illustrates the magnified fractured surface, with one fracture occurring directly on the rays' patches and another fracture on the region with alternating grain direction.

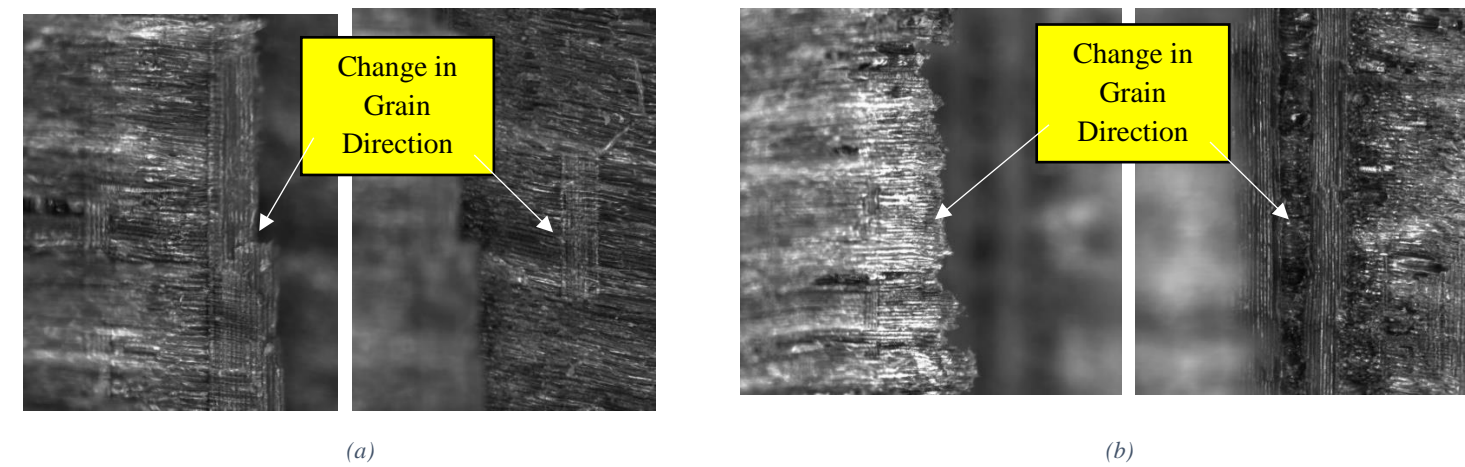


Figure 3.1.2 - 2: (a) Fractured Surface Magnified 8x, (a) On the rays' patch. (b) On the contacting region of rays' patches and fibres.

3.2 Material testing

3.2.1 Aim and Objectives

The primary aim of the bend and tensile tests is to identify and characterise features acting as stress concentrations within wood veneer samples. This information is vital for understanding the material's failure susceptibility and guiding decisions regarding its application and processing. To achieve this aim, the tests will focus on the following objectives:

- Perform bend tests on various samples and analyse the results to identify contributing features to failure.
- Measure and record the tensile strength and failure strain of the veneer to establish baseline mechanical properties. Significant variations across different specimen locations may indicate areas of weakness.
- Examine the fracture surface post-test to determine the failure mode and potential crack initiation points, with an expectation of a brittle failure mode.
- Compare results from multiple specimens to assess consistency and identify systemic issues within the material.
- Test multiple veneer samples from different locations to evaluate the extent of observed weaknesses and determine if they are isolated occurrences or indicative of broader issues.

Various testing schemes were planned and executed to achieve the aims, focusing on bend and tensile tests to identify stress-concentrating features through failure under different stress types and loads expected in the manufacturing process. Samples were maintained at atmospheric conditions to minimize moisture content variability's impact on the data, ensuring consistent results for feature identification. The collected data from these tests will facilitate the differentiation between strong and weak samples, aiding in the characterization of concerning features.

The three-point bend test enables bending to failure with a focused load, providing quantifiable data on load and displacement for different samples. Conversely, the Cake Tier bend tests distribute the load more evenly, offering insights into the specific features causing failure. This combination of testing methodologies allows for a comprehensive understanding of stress concentration mechanisms within the wood veneer samples.

3.2.2 Bend tests

Research was conducted to explore various testing methods for evaluating wood veneer samples, with bend tests emerging as a highly promising approach aligned with the project's objectives. Drawing insights from studies by Lunguleasa et al. [2] and alternative investigations by [3], two types of bend tests were selected for implementation. While the project's focus was not on assessing the material properties of the samples, these bend test methods proved valuable due to their ability to simulate stresses like those experienced during manufacturing processes. As such, the failures observed in these tests are expected to mirror common failures encountered in the stakeholder's forming process, thereby providing relevant insights into stress concentration mechanisms during manufacture.

3.2.2.1 Three-point bend test

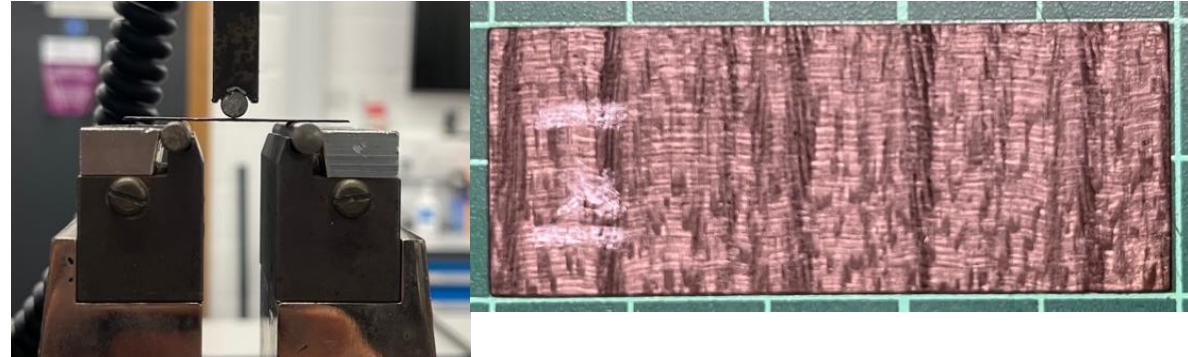


Figure 3.2-2: Left: Three-point bend test set up in Instron machine. Right: Example of sample used in test

The methodology for the three-point bend test involved cutting a set of 25 samples from a veneer piece and testing them using an Instron electromechanical machine. These samples were laser cut to dimensions of 20 x 50mm, oriented perpendicular to the longer side of the whole veneer piece. The samples were then loaded on a three-point bend apparatus with a 20mm diameter between supports and a load applied at the centre. Testing was conducted at a head speed of 1mm/min with a 500N load cell, and tests were stopped at a maximum displacement of 6mm using Instron software.

Prior to testing, the samples were categorized and photographed for analysis. Results from 20 samples were recorded, with 5 additional samples used to set the expected critical displacement. Analysis revealed a range of failure loads (3.2-8.4N) and displacements (4.6-5.7mm), with samples ranked accordingly. Higher load failures were associated with grainier textures or shorter ray structures, while lower load failures occurred in samples with longer rays, as observed in Figure 4.

To confirm findings, binarised images of the samples were analysed, aligning with the proposed feature detection code's process. While load variations were evident, no clear displacement trends were observed. Additional tests at

90 and 45 degrees did not result in failures, indicating no concerns with bending in these orientations. Further tests were planned to better understand stress concentrations in the material.

3.2.2.2 Cake Tier Apparatus Tests

The cake tier test involved bending wood samples around varying radii to simulate a distributed load and identify failure points. Similar to the three-point bend test, a set of 25 samples were prepared to dimensions of 50mm x 20mm using a laser cutter, then photographed and categorised for analysis post-bending. The cake tier apparatus, displayed in **Error! Reference source not found.**, comprising tiers labelled T1 through T6, was manufactured using 3D printing. The tiers have varying diameter, with T1 having the largest diameter, and T6 having the smallest diameter. The diameters chosen were based on maximum deflection calculations from the three-point bend tests.

Initially, samples were bent by hand as they had been conducted in Lunguleasa et al. [2], but the use of brackets was adopted for improved repeatability and consistency. The first 10 were bent by hand while the further 15 were bent using the brackets. Observations were made regarding sample failures and features such as ray length variations. Results indicated that longer rays and variations in ray lengths contributed to weaker samples, aligning with findings from the three-point bend test. The findings of these tests can be found in Appendix A.

Further tests were conducted for 45 and 90-degree orientations, revealing similar trends of extreme bending without failure. Minor surface cracks were observed in some 45-degree samples but were deemed negligible. This is as during the veneer forming process, the veneer would be pre-treated for moisture content and heated, which would improve the ductility of the wood veneer.

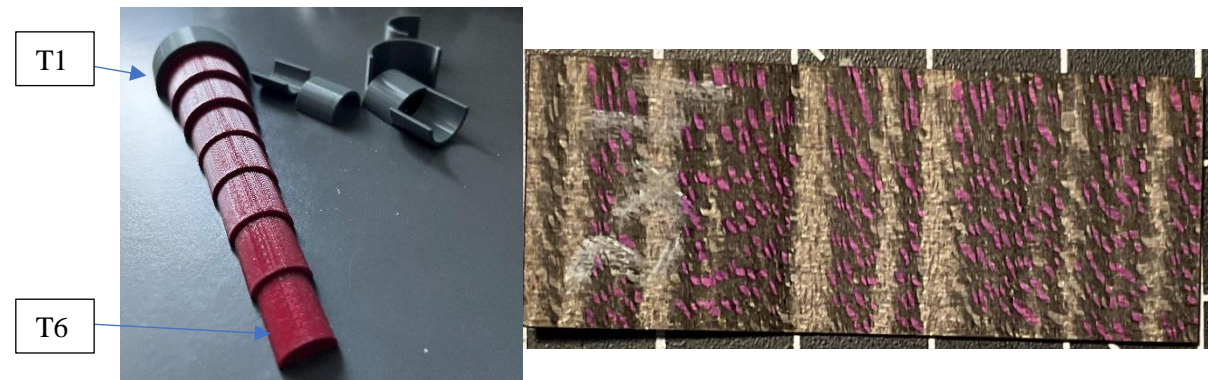


Figure 3.2-1: Left: cake tier apparatus with brackets, right: Sample with rays highlighted.

Overall, the three-point bend test did not reveal a conclusive trend in displacement, but it did identify a pattern in the force applied to the samples. Specifically, samples with longer rays tended to fail at a lower load compared to those with shorter rays. Therefore, to further validate this observation, the cake tier apparatus test was conducted, simulating the forming process more accurately. Both tests corroborated each other's findings, while further confirming that variations in ray length could lead to failure at a lower bending radius than anticipated.

3.2.3 Tensile tests

3.2.3.1 Methodology

The experiment setup, depicted in Figure xx, utilizes the Instron 5569 test machine for conducting tensile tests on wood veneers. Serrated wedge grips were chosen for their gripping force and suitability for flat materials, with dimensions tailored to fit the grip areas of the veneer specimen. Rubber squares were affixed to prevent crushing of the veneers by the grips. The specimen was securely mounted, ensuring proper alignment and precise centering of the gauge length within the grip opening. Displacement control was selected as the test mode, commonly used in tensile testing and suitable for this experiment. The specimen protect function was enabled during grip tightening to prevent

excessive force application. A 50 kN load cell, exceeding the anticipated tensile strength of the veneer, was employed. Additionally, the test automatically terminates upon detection of sudden force changes indicative of specimen fracture. An extensometer was utilized for high-precision strain measurement during the test.

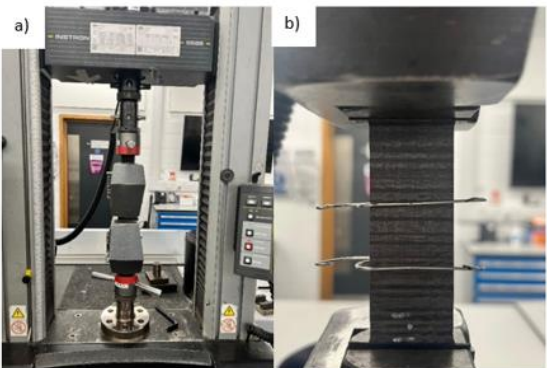


Figure 3.2.4-1: a) Set up of Instron 5569 test machine for tensile test, b) Extensometer clipped on to the gauge section of the veneer during the test

3.2.3.2 Result and discussion

Table 2.3-2: Results obtained from the tensile test for specimen orientation of 0°, 45° and 90°.

Specimens Orientation	Strongest sample	Weakest sample	Range of ultimate tensile stress (MPa)	Average ultimate tensile stress (MPa)
0°	Sample 1.3	Sample 2.3	12.303-21.068	17.592
45°	Sample 4	Sample 5	8.86-12.29	10.8
90°	Sample 6	Sample 4	6.57-9.26	7.884

Table 3.2-1. Tensile Test Results

From Table 3.2-1, it can be observed that for 0° orientation, Sample 1.3 is the strongest sample and Sample 2.3 is the weakest sample. On the other hand, from it can be observed that for 45° orientation, Sample 4 is able to withstand the highest ultimate tensile stress, whereas Sample 5 is able to withstand the lowest tensile stress. Lastly, it is observed that for specimens that were laser cut in 90° orientation, Sample 6 is the strongest sample, whereas sample 4 is the weakest sample. This is due to the sample was laser cut from different piece of veneer and another reason which would cause the difference in the value could be due to experimental error, for example: the specimen may not be perfectly straight when it was clamped on to the machine which would cause the sample to bend slightly during the tensile test. After comparing the average ultimate tensile stress of specimens which were laser cut in different orientations it is found that specimens which were cut in 0° is the strongest orientation, whereas specimens which were cut in 90° is the weakest orientation. This has proven the previous hypothesis from the microscopy test to be correct that the specimen will be strongest when it is pull in parallel direction of the fibres of the veneer.

The use of high-speed camera is implemented to capture and identify the precise location and characteristics of crack initiation in wood veneer. Due to data storage and limitation of the camera higher frame rate was not implemented in the experiment. Therefore, the frame rate was set to 150 fps. Proper lighting was setup for the camera. However, the frame rate of 150 fps could not capture the initiation and early stages of crack propagation in the veneers. Figure 4.3-1 illustrates the image capture by high-speed camera during the tensile test and the region highlighted in red indicates the fracture point.

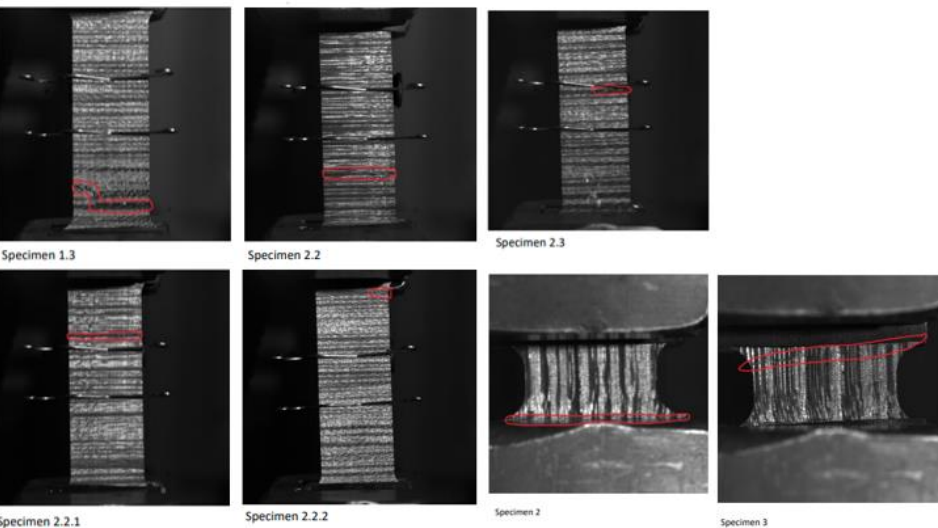


Figure 3.2.3 Image capture by high-speed camera during the tensile test.

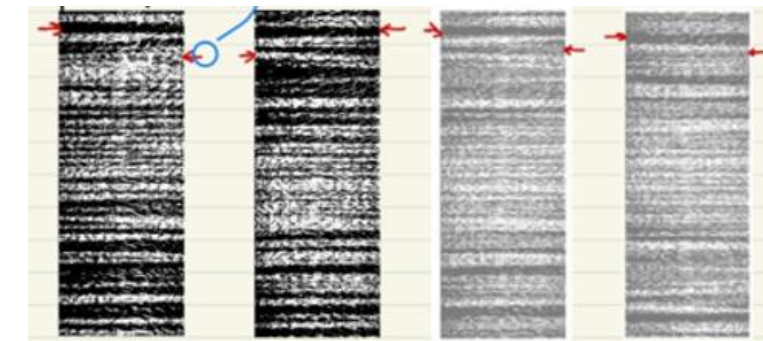


Figure 3.2.4. Image capture by high-speed camera during the tensile test.

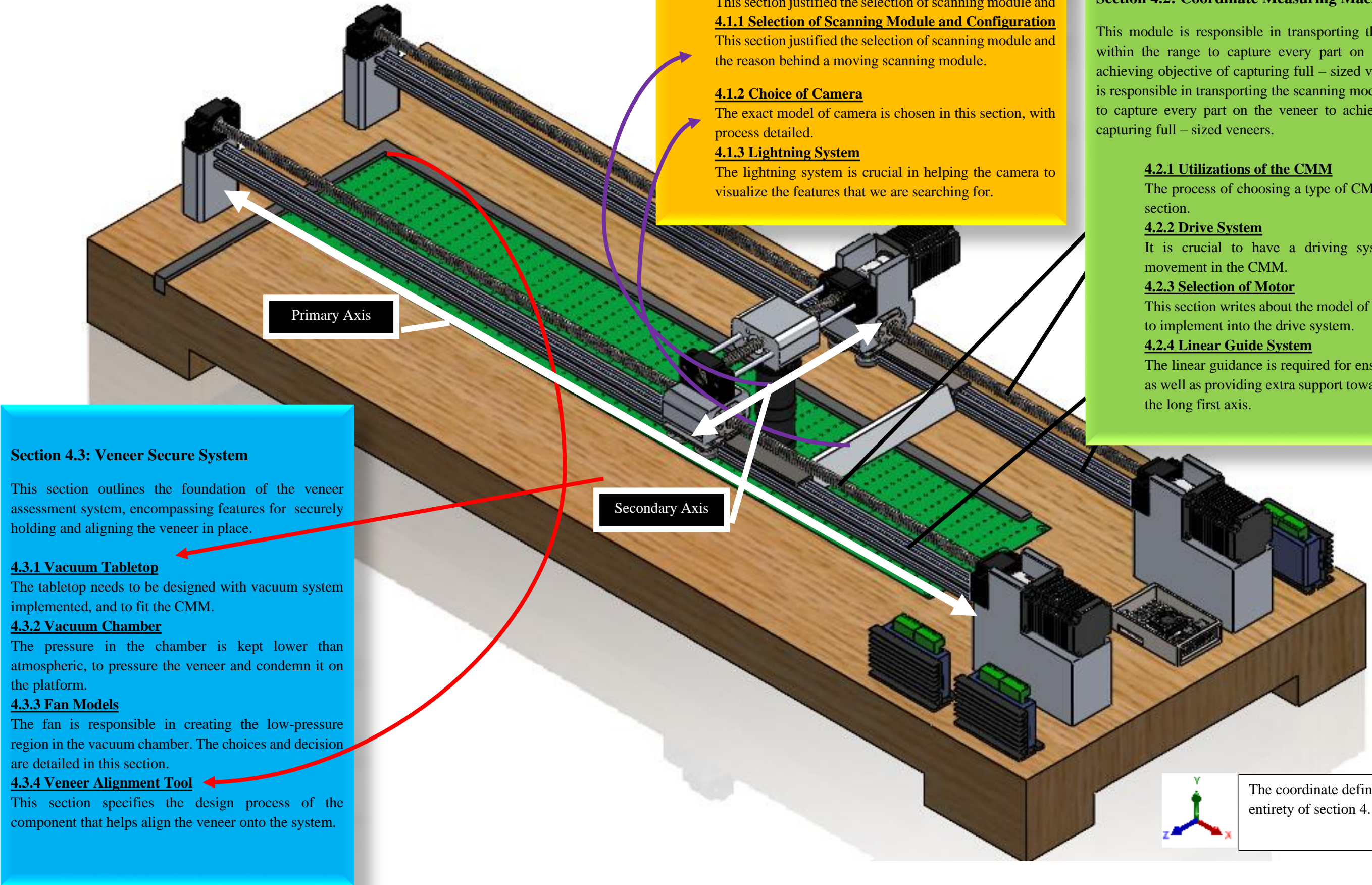
Furthermore, analysis of the binarized image for 0° orientation were done and illustrated in Figurexx. Our analysis revealed that overlapping the front and back images effectively reduces the number of black stripes present and cracks tended to occur in regions with a higher concentration of black stripes. Moreover, it is also observed that a clear distinction between the texture of the strongest and weakest samples. The weaker samples exhibited a characteristic with longer and more prominent rays in their texture and vice versa.

In general, it is observed that that specimens which were cut in 0° is the strongest orientation, whereas specimens which were cut in 90° is the weakest orientation as it is pull in parallel direction of the fibres of the veneer. From the binarized image it is concluded that weaker samples exhibited a characteristic with longer and more prominent rays in their texture which correlates with the finding of the bend test.

3.2.4 Conclusion of tests

The purpose of these tests was to locate features in the wood structure that act as a stress concentrations and lead to weakness in the samples. From the three-point bend test no conclusive trend could be found in the structure for the displacement but a trend in the force applied to the samples was found. Samples with longer rays present in the structure would fail at a lower load than those with shorter rays. To confirm this hypothesis, further tests were proposed with a testing method more reflective of the manufacturing load the veneers would be subjected to. These tests were conducted using the cake tier apparatus and the hypothesis from the three-point bend test was confirmed with an added finding that the variation of ray length in a sample would cause it to fail at a lower bending radius. These results were compared with the results of the tensile tests to validate the findings and have a higher confidence in the results. Across all testing types, the significance of the ray lengths in relation to the strength of the part were consistent and therefore it can be concluded that this is the feature of concern. This information was passed to the image analysis team to tailor the detection algorithm.

4 Hardware



4.1 Scanning Module

4.1.1 Selection of Scanning Module and Configurations.

The initial conceptual ideas (**Error! Reference source not found.**) proposed by the team led to three primary configurations of scanning modules to be considered. In which, some configurations involve modules that move to scan the platform, while others entail the platform moving towards the module's projection. Additionally, there were designs where both the platform and the module remain stationary. After thorough discussions, it was concluded that creating a moving platform would be complex, given limited payload capacity and additional space requirements. Moreover, the risk of inaccuracy due to misalignment with the scanning modules prompted the team to exclude this approach from further consideration in the tally matrix.

The criteria were assigned based on the stakeholder demands, team priorities, and indirect stakeholders needs. A weighted matrix was not utilised as each evaluation criteria is of equal importance. Instead, a tally matrix ranks each evaluation criteria from a scale of 0 to 5. The team priorities, which are shown in black, prioritises the desired physical attributes of the scanning module, while indirect stakeholders need, highlighted in blue, correspond to the safety criteria, environmental concerns as well as requirements for virgin resources. The stakeholder requirements relate to criterions that are highlighted in red.

Scanning Module Configurations		
Evaluation Criteria	Moving Scanning Module	Fixed Scanning Module
Data Consistency	5	0
Versatility for Veneer Size	5	0
Environmental Considerations & Material Usage	3	5
Safety (EN ISO 12100)	4	5
Versatility in Adjusting Resolution	5	0
TOTAL	22	10

Table 4.1-1 Tally Matrix of Scanning Module Configurations

Based on Table 4.1-1 Tally Matrix of Scanning Module Configurations **Table**, the moving scanning module was chosen as it met majority of the criteria. The moving scanning module achieved a 5 in data consistency, where the fixed achieved a 0. This is due to the moving scanning module having the ability to shift positions to ensure that veneers that are larger than the camera's projection size can be reached. This also corresponds to the resolution versatility, as any imaging evaluations from the scanning module that were unclear could be repositioned to create a clearer image. Both criterions correlate to the veneer size versatility criteria, as the moving scanning module would have more versatility with different sizes of veneer in comparison to a fixed one.

The moving scanning module presents challenges in terms of environmental impact, as it typically requires more materials compared to a fixed mechanism. However, this drawback would be later mitigated by incorporating recyclable materials into the design process. Additionally, there were safety concerns associated with a moving scanning module, although the risk of injury is minimized since the machinery will not be operating at high speeds. Consequently, the team is exploring various types of scanning modules, as detailed in Table 4.1.1-2.

Choices of Scanning Module					
Evaluation Criteria	Camera	X-ray	Air-Coupled Ultrasound Device	3D Scanning LIDAR	Laser Scanning
Form Factor	4	2	3	3	5
Availability in Market	5	3	2	2	5
Initial Cost	5	2	1	2	1
Resolution	4	5	2	3	4
Implementation Simplicity	5	2	3	3	3
Safety	4	1	4	4	2
Applicability to Veneer	5	2	3	1	3
TOTAL	32	17	18	18	23

Table 4.1-2 Tally Matrix of Scanning Module Options

After thorough evaluation, the camera emerged as the most favourable choice among the options, meeting most of the criteria with scores of 4 or above across the board. Its ready availability in the market, combined with its relatively compact size and diverse range of models, allows for seamless integration with other subsystems without spatial constraints. Furthermore, the initial cost of a camera is lower compared to other alternatives, while still providing a resolution comparable to that of the laser scanner.

Several studies have showcased the effectiveness of high-resolution CCD cameras for wood defect recognition, achieving a point-to-point sampling distance of 3.1mm at 10m from the scanner [4]. In contrast, laser scanners, as observed in a separate study assessing log geometry and wood quality, attained a resolution of approximately 40 points per 25mm around the log circumference [5]. While although X-ray technology excels in resolution, its limited applicability to wood veneers limits its utility in this context.

The camera's suitability for wood veneers was well-documented in numerous studies, particularly in surface assessments of wood panels which were often paired with visual inspection algorithms. For instance, the implementation of a faster region-based convolutional neural network (faster R-CNN) in identifying defects on wood veneer surfaces achieved an impressive accuracy of 96.1% [6]. Conversely, the utilisation of LIDAR technology on wood veneers remains rare, primarily reserved for forestry applications such as deforestation control and precision forestry [7]. Ultrasound, typically employed for dyeing veneers, finds limited application in this context [8], [9].

In conclusion, the camera emerges as the superior choice due to its fulfilment of most criteria and proven applicability to wood veneer projects. Its ready availability in the market and lower initial cost makes it an attractive option for prototyping, while its relatively high resolution ensures consistent and reliable results.

4.1.2 Choice of Camera



Figure 4.1-1: Image Captured using Conventional Camera.

Under 2x magnification from the microscope, ray patches are clearly visible and distinguishable, providing a reference for selecting the camera module model. Using a conventional phone camera with 12MP resolution, 1/2.55" sensor, 1.4 μ m pixels, and f/2.2 aperture lens, it was found that a 1.7x magnification and a distance of 30 mm from the object were sufficient to visualize the patches. An example of a veneer image captured with the conventional camera is displayed in **Figure 4.1-1**. The primary criterion for selecting the camera module was its capability of integration with Raspberry Pi, as depicted in **Figure 4.1-3**.

After careful evaluation, the Raspberry Pi HQ Camera Module emerged as the optimal choice. The reasons leading to the disqualification of other modules, these reasons would be:

- Low Resolution/Lack of ability to capture video.
 - A higher resolution would be needed to capture the features in greater detail.
 - Videos would provide an alternative veneer surface imaging option.
- Lack of Auto Focus
 - Reduces human interaction with the imaging system and allows for an automated process.
- Lack in Zoom Capability
 - A zoom would be required to focus in on the features of interest.
- High minimum object distance (M.O.D)
 - In the requirements, also, having camera module higher introduces additional structural instability.



Figure 4.1-2: Raspberry PI HQ Camera Module

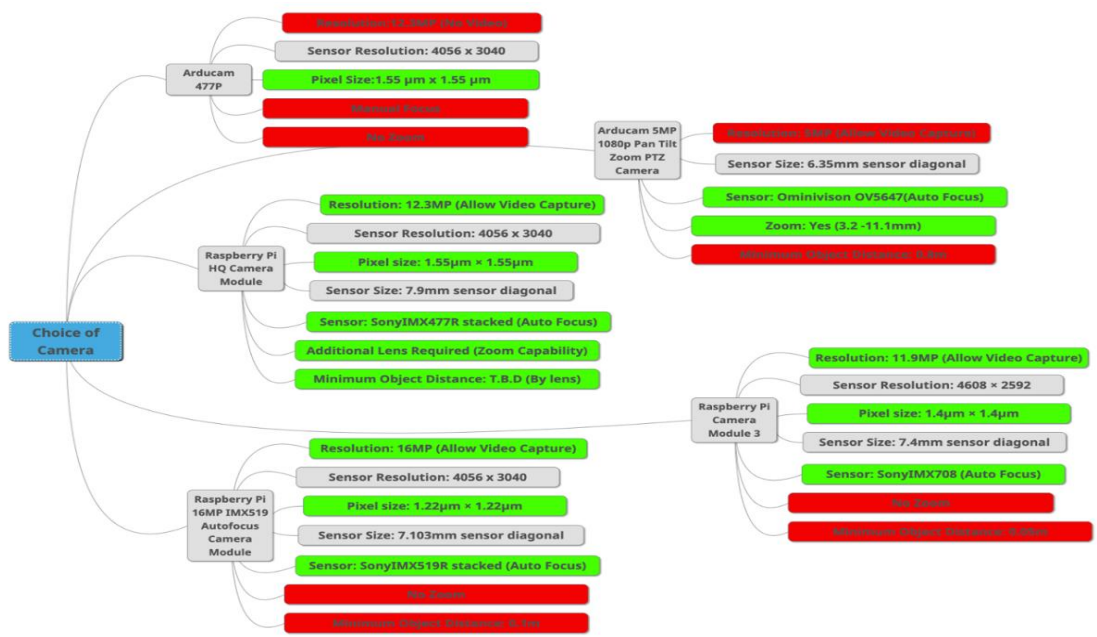


Figure 4.1-3: Mind-map of choice of camera.

Notably, prioritizing a magnifying camera module (Zoom Capability) over physically shortening the distance between the object and the camera module is advantageous. This is as attempting to physically shorten this distance within the system design would necessitate the design of a mechanism to move in the z-axis, introducing additional variables and uncertainty into the system, potentially affecting overall system stability. Moreover, vertical movement of the scanning module relative to the ground could interfere with the lighting system, leading to the risk of shadow casting onto the veneer, interrupting the imaging process. Therefore, the magnifying capabilities of the camera module emerged as one of the primary considerations in the selection process.

When considering the lens for the camera module, several factors are critical:

Figure 4.1-4: Pimoroni 100x Industrial Microscopy Lens.

- **Zoom capability:** Ensuring the lens has zoom capabilities allows for focusing on specific areas of interest with precision, enhancing the detail captured.
- **Ability to focus on low object distance:** Essential for the lens to focus effectively on objects at a close distance, particularly for capturing fine details on the wood veneer surface.
- **Limitation of resolution from the lens:** Lens should not introduce limitations on the resolution of the captured images, ensuring high quality visuals for accurate analysis and defect detection.

The Pimoroni Microscope Lens emerges as the most suitable design option, as depicted in **Figure 4.1-4**. Unlike other lenses considered, such as the Raspberry Pi High Quality Camera Lens or the C-Mount 8-50mm Zoom Lens, the Pimoroni lens is specifically engineered for microscopic applications. It excels in focusing on short distances, with a range from 2.4 to 36mm, meeting the design requirements effectively. Additionally, its optical zoom capabilities, ranging from 0.12x to 1.8x, fulfilling the specified zoom criteria with precision.

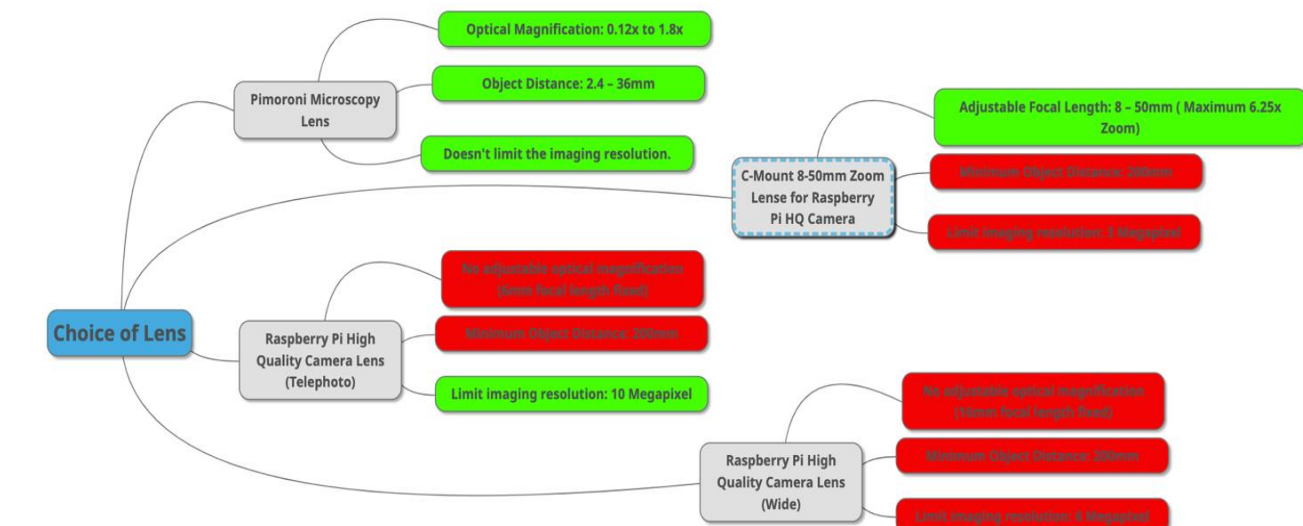


Figure 4.1-5: Mind-map for choice of lens



4.1.3 Lighting System

It was mentioned in the camera selection section, that it is imperative to acknowledge the veneer's sensitivity to lighting conditions, which could substantially alter its visual appearance. Therefore, a consistent lighting setup must be meticulously designed and incorporated to ensure that the images captured are uniform and recognizable by the feature detection algorithm.

In investigating the lighting specifications, the following key parameters will be considered:

- Colour Temperature:** Selecting the appropriate colour temperature to accurately represent the colours and textures of the wood veneer, ensuring optimal visual clarity and fidelity.
- Brightness:** Determining the ideal level of brightness to uniformly illuminate the veneer surface while avoiding overexposure or underexposure in the captured images.
- Orientation and Angle:** Assessing the optimal orientation and angle of the lighting sources to minimize shadows and ensure even illumination across the veneer surface, enhancing feature visibility and analysis accuracy.

Figure 4.3.1-2 illustrated the effect on altering the orientation of the light source. The figure is captured using similar setup used as the above Section 4.1.2 when investigating the camera. It was demonstrated that the lighting orientation affects the appearance of the ray patches and the fibres, which revealed that the lighting orientation (description of orientation of light in *Error! Reference source not found.*) influences the appearance of both the ray patches and the fibres, causing one to appear darker than the other in certain orientations. The difference between this veneer appearance under different lightning angle is minor, hence the only consideration for the angle is that it needs to be setup such that all the rays appear to be identical in colour under optical camera.

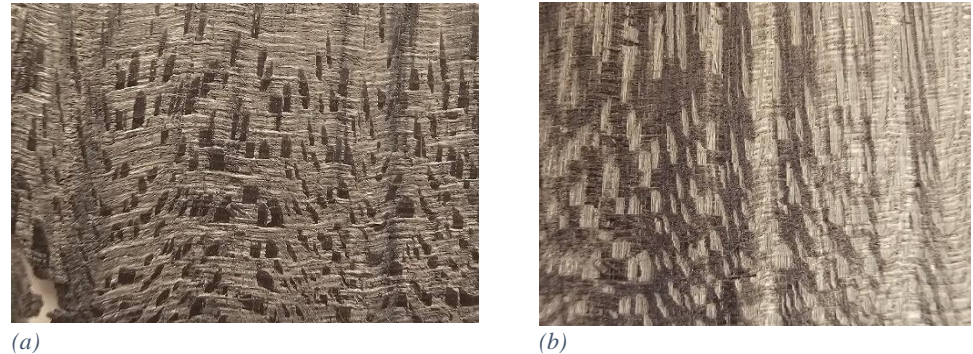


Figure 4.1-7: Appearance of the Veneer (a) Light shining perpendicular to the fibres' grain direction (from the top). (b) Light shining parallel to the fibres' grain direction (from the right).

The distance between the light source and the veneer would also alter the local luminous intensity of same region specifies above. A reversed behaviour of the colour can be observed when the light source is placed closely to the veneer. It is also evident (*Appendix B - 2*) that placing it too close to the veneer introduce an over-exposed region on the image, in which no feature can be visualized.

Following investigation regarding the colour temperature, using diffuser with white, red, blue, and yellow were conducted (*Appendix B - 3*). It was found that white and yellow diffusers outperformed others, with the difference between the white and yellow diffuser being minor. As such, it was decided that a white diffuser would be chosen. Additionally, a luminous intensity of 1000 lumens were determined to adequately illuminate features for visualisation. These findings inform the lighting requirements of the system.

The lightning requirements obtained are as follows:

- Angled at 30-60° to cover the veneer based on the distance of the light horizontally and vertically from the veneer.
- Positioned 7cm horizontally from the veneer.
- Positioned 5cm vertically above the veneer.
- White light and diffuser (Colour temperature of 5600-6000K).
- Achieving a luminous intensity of 1000 lumens.



Figure 4.1-6: (a) Conceptual Design. (b) Design 1. (c) Final Design

Figure 4.1-6 illustrates the design process of the lightning system. The initial conceptual design incorporates a slider and hinge mechanism to adjust the distance and angle of the light source, respectively. It is intended to be placed on the base, with the light source positioned parallel to the x-axis (referencing page 9), thereby shining perpendicular to the y-axis. However, as the requirements are established, this design is eliminated.

Moving towards design 1, as illustrated in **Figure 4.1-6(b)**, the orientation of the light remains similar to the conceptual design. The red box highlights the component to be slotted into the bottom, empty column of the v-slot, which then secures the light strips platform. The platform holder is designed to allow for 360-degree rotation of the light strip platform, enabling precise control over the angle of illumination.

This design was soon discarded due to a potential issue identified by the software part, which suggested that the code could identify the rays' patches better under the condition of **Figure 4.1-6(b)** than in (a). Hence, the orientation of the lighting needed to be changed to shine parallel to the grain direction of the wood fibres.

Figure 4.1-6(c) illustrates the final version of the lighting system, representing a refined design that ensures seamless integration and optimal functionality. The lighting system comprises a platform holder with a hook and a light strip platform. This platform holder sits atop a V-Slot linear rail system and is attached to the gantry plate using the hook. This configuration enables the lighting system to slide smoothly together with the camera for precise positioning. The light strip platform, attached to the platform holder, provides a stable mounting point for the light strips. Crucially, this platform allows for 360-degree rotation, facilitating flexible control over the direction of illumination. In summary, the system offers secure light bar mounting, a mobile platform for moving the light strips together with the camera, and adjustable angle for the light.

The final selected strips that adhere closely to the specification will be the Ultra LED, with other options illustrated out in Figure 4.1.3 - 3. The criteria of "integration towards Raspberry Pi" not being prioritised in this matter, as the correct requirements is more important in visualising the features. Hence, although the Ultra LED cannot be integrated directly to the Raspberry Pi, it is still selected to be the best choice. Notably, another strip, WS2815B demonstrated high flexibility and tolerance towards future modifications. It is known by now that some veneers' visual appearances are sensitive towards the lightning condition. Considering other type of veneer that might requires a higher light intensity or different colour temperature, introducing a two light strips setup instead of one increase the inclusivity of our system. Thus, the ability of WS2815B to vary its colour temperature, and ease to integrate into the Raspberry Pi makes it the best choice to be implement into the system as a secondary strip.

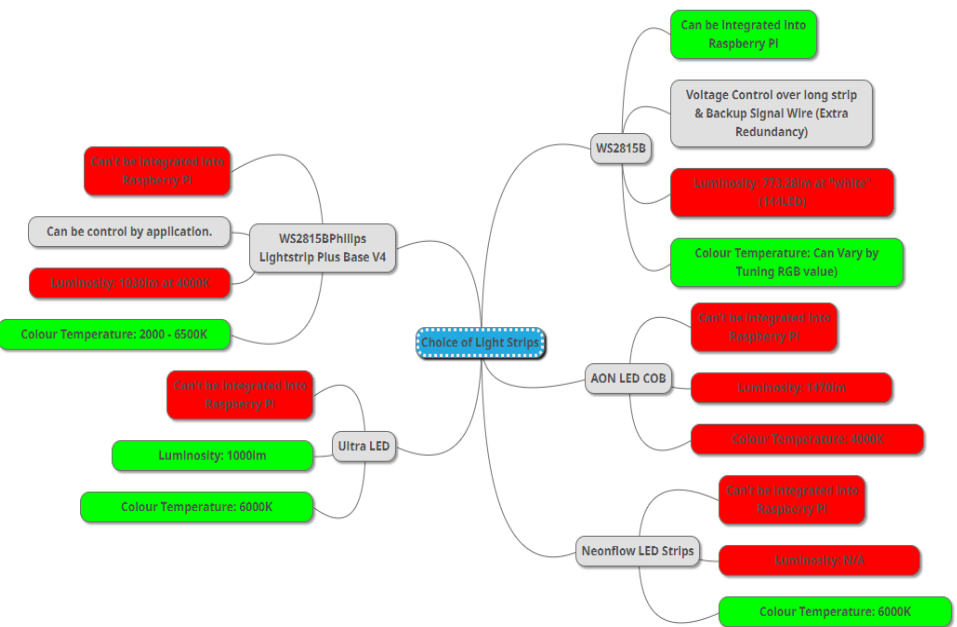


Figure 4.1.3 - 1: Mind-map for choice of light strips.

4.2 Coordinate Measuring Machine (CMM)

4.2.1 Usage of Coordinate Measuring Machines (CMM)

As established, a moving camera will be utilised for the final design. Initially, ideas revolved around implementing a motion mimicking a 3D printer to manoeuvre the scanning module. 3D printers typically use a configuration or a form of a coordinate measuring machine, in the application of moving the camera at a precise manner to position itself across the wood veneer, opting for a coordinate measuring machine (CMM) will be the most practical solution. The nature of a CMM being able to track the coordinates of its moving probe also benefits the data analysis team in locating regions of weakness at specific points of the veneer. The main stakeholder requirement that the coordinate measuring system evaluates is the veneer size.

Choice of CMM (Coordinate Measuring System)				
Criteria	Moving-bridge CMM	Fixed-bridge CMM	Gantry CMM	Cantilever CMM
Accuracy	5	5	3	1
Safety (ISO 12100)	5	5	5	5
Stability and Rigidity	5	5	5	3
Size and Space Coverage	1	1	5	4
Environmental Considerations and Material Usage	3	3	2	5
Flexibility for future modifications	0	0	5	4
TOTAL	19	19	25	22

Table 4.2-1. Tally Matrix of CMM Types

Overall, according to the total scores in the tally matrix, shown above in **Table 4.2.1-1**. The Gantry CMM emerges as the optimal choice as it demonstrates superior stability, rigidity and offers flexibility for future modifications. [10]. Despite having a relatively lower accuracy than the moving and fixed bridge CMMs, the gantry CMM has a decent amount of accuracy. Where bridge CMMs can achieve an accuracy of $\pm(0.3 + L/1000)\mu\text{m}$ [11], where L is in mm. the gantry CMM achieves an accuracy of $\pm(7 + 8L/1000)\mu\text{m}$ [gantry]. This accuracy is sufficient for the application of assessment of veneers, with each image taken can be overlapped by a margin of at least 10% with this accuracy. Adding to that, the accuracy can be improved with the selection of a drive system, where the options are later discussed in the report. The stability of bridge and Gantry CMMs surpasses the

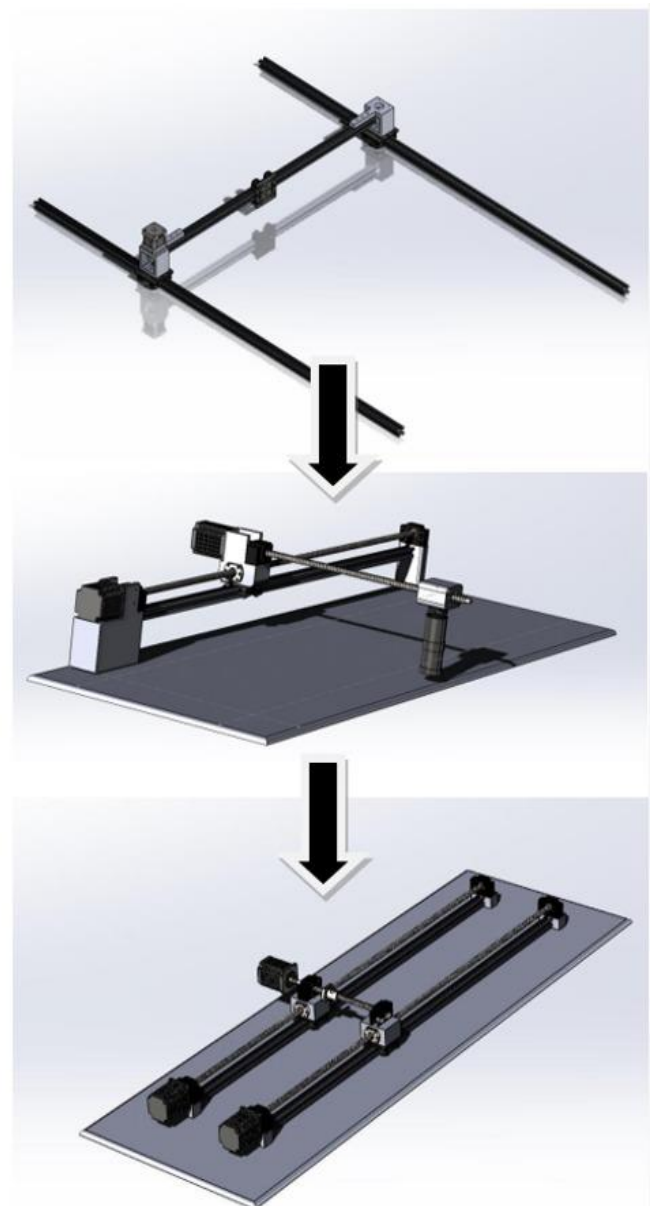


Figure 4.2 - 1: Conceptual Designs of the CMM.

cantilever configuration, as they are supported by a minimum of two pillars, whereas the Cantilever only had one. Having stability on the CMM is essential to ensure that the coordinates of the system does not alter after periods of usage. To satisfy the versatility criteria from the primary stakeholder, the CMM must cover a space as large as 720mm x 125mm. However, the bridge configurations will require a base which stems across the size of 720mm x 125mm minimum, to obtain the required space coverage, this not only increases wasteful usage of materials. It also creates complications in the moving mechanism. On the other hand, the cantilever and gantry configurations can be extended via its axis arms to fit the space requirement. The Gantry falls short on the environmental concerns, as it utilises more materials than other configurations, this leads to a potential of utilising more virgin resources. However, it has the most flexibility for future modifications, as each axis arm can be detached to be upgraded with a different drive system or material.

4.2.2 Motion System

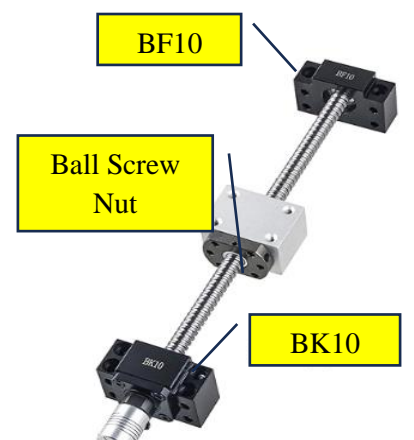
In Table 4.2.2, options suitable for the application of a fitted camera in the coordinate measuring machine's motion system are presented. Drive systems like pneumatic actuators and piezoelectric motors are excluded from consideration due to their scale-specific usage. Pneumatic actuators find typical application in larger domains such as railways and aviation [12], while piezoelectric motors are commonly employed in microscopic settings, including disk drives and microscopy.

The power efficiency criterion, denoted in blue, holds importance as an indirect stakeholder priority. Enhanced power efficiency plays a pivotal role in addressing environmental concerns, with higher efficiency resulting in reduced overall energy consumption.

Drive Systems for Linear Motion System				
Criteria	Motor Less Systems (Will require a driving force)			
	Lead Screw	Ball Screw	Belt and Pulley	Rack and Pinion
Power Efficiency	3	4	4	4
Initial Cost	5	4	4	2
Life Expectancy of System	3	4	3	1
Weight	3	2	3	1
Versatility for Veneer Size	5	5	3	5
Safety (EN ISO 12100)	3	5	3	1
Resolution	4	5	2	3
TOTAL	26	29	22	17

Table 4.2-2. Tally Matrix of Linear Motion Systems

According to **Table 4.2.2-1**, the power efficiency of a ball screw rivals that of other motorless systems except for the ball screw itself. Systems like the belt and pulley, and rack and pinion typically achieve over 90% efficiency [13], [14], [15]. The initial costs of ball screws are like belt and pulley and rack and pinion systems. However, lead screws are costlier due to their simpler construction. Ball screws boast the highest life expectancy among these systems. Lead screws and rack and pinion systems suffer from high friction,



whereas belt and pulley systems wear out over time, leading to reduced resolution and potential backlash issues. This could affect image overlapping in cameras. The ball screw has reduced friction due to the loaded ball bearings in the shaft, which replaces the sliding friction between the shaft and the rod with a rolling friction, which has less resistance and generates less heat. Ultimately increasing the longevity of the system. The resolution of lead screws and rack and pinion

Figure 4.2.2 - 1: SFU1204 ball screw with BF10 and BK10. [online]

systems is approximately 0.00278 mm° and $0.436332222 \text{ mm}^\circ$ respectively [16], [17], while ball screws offer a resolution of approximately 0.01389 mm° [18]. Ball screws and rack and pinion systems are lighter due to usage of minimal steel. Ball and lead screws offer greater versatility in accommodating different veneer sizes by adjusting their length. Safety concerns include finger pinching with rack and pinion systems and friction-related injuries with belt and pulley systems. Ball and lead screws are safer due to their slower movement speed.

In summary, ball screws emerge as the preferred choice for drive systems due to their superior power efficiency, longevity, and reasonable initial costs. Despite being heavier, they offer excellent adjustability for different veneer sizes and comply with ISO 12100:2010 safety standards.

A smaller diameter ball screw allows faster movement for the CMM and reduces the motor's load. A smaller pitch gives, higher precision, given a fixed step size from the motor. Hence, the best option will be to choose the one with smallest pitch and diameter. With the standard ball screw range from 12 – 20mm for diameter and 4 – 10mm for pitch size, the best option here is the SFU1204, which consists of diameter of 12mm, and pitch size of 4mm. It is made fully metal, mainly steel and aluminium, thus all recyclable, and sustainable. With all that combined, it is no doubt the best design option in achieving the objective to translate the scanning module to identify the concerning features on the veneer.

4.2.3 Selection of Motors

Choice of Motor						
Evaluation Criteria	Stepper Motor	Brushless DC Motor	Brushed DC Motor	AC Motor (Induction Motor)	Servo Motor	Spur Gear Motor
Initial Cost	5	1	4	3	2	4
Weight	4	5	3	2	2	3
Torque	5	5	5	5	5	3
Power Efficiency	3	5	5	5	5	5
Life Expectancy of System	5	4	1	5	4	4
Integration within Raspberry Pi	5	3	3	1	5	2
Resolution of Motor	5	3	3	1	3	2
TOTAL	32	26	24	22	26	23

Table 4.2.3 - 1: Tally Matrix of Motor Choices

The initial cost of a stepper motor is lower than the rest of the motor choices. It also has a relatively low weight in comparison to the rest of the motors. All motors except for the spur gear motor supplies torque proportional to the current supplied, hence it is rated at the highest as the only limitations will be dependent on the specific model of the motors. The spur gear motor's torque is dependent on the input torque and the gear ratio. The power efficiency of the stepper motor is relatively lower than the other motors, with an efficiency around 40-50% [19], [20]. Whilst the rest of the motors can achieve a power efficiency often around 80% and above.

The model chosen for the stepper motor is the NEMA23 (specifically 23HE4S–2804S). The typical torque range for the stepper motor is listed as **Table 4.2.3 - 2: Typical torque range for stepper motor**. This is chosen by doing a weight estimation (in **Table 4.2.3 - 3**) of the overall system, to ensure the torque of the motor can be sufficiently handle the weight of the system. The step size of the motor comes with either 0.9 or 1.8deg. The trade-off of a smaller step size, which gives higher precision, is the significant reduction in torque and increment in cost. It is also calculated that when coupled with a ball screw model SFU1204, the difference of step size when translated into linear motion is minor, with 0.01 and 0.02mm per step respectively.

Stepper Motor Form Factor/Model	Torque Range (Nm)
NEMA 17	0.5 – 0.7
NEMA 23	1.0 – 4.0
NEMA 34	12

Table 4.2.3 - 2: Typical torque range for stepper motor.

Component Name	Amount	Per Weight (kg)	Total Weight (kg)
SFU1204 (1000mm)	2	2	4
SFU1204 (500mm)	1	1.32	1.32
23HE4S–2804S	1	1	1
Connector Blocks (Aluminium)	3	0.446	1.338
Raspberry Pi HQ Camera Module	1	0.015	0.015
Pimoroni Microscopy Lens	1	1 (Approx.)	1 (Approx.)
<i>Total Weight:</i>			8.7

Table 4.2.3 - 3: Weight Estimation.

Translating the total weight into torque using **Eqn 4.2.3 – 1**, the minimum requirement for each motor is found to be approximately 0.53Nm of torque.

$$T = 0.5 \times \text{Diameter} \times \text{Weight}$$

Eqn. 4.2.3 - 1

Considering the torque curve goes down with rpm quite significantly [21], a torque two times higher than the minimum requirement would be reasonable to ensure smooth and fast movement, and thus a NEMA 23 stepper motor is chosen as the optimal design option in this concern.

Notably on the main, longer axis on the CMM, it is selected to include one motor each side, to ensure simultaneous and consistent motion on both sides, disabling any disjointed movement that will cause the scanning module to be slanted.

4.2.4 Utilisation of a Guide System

The nature of a ball screw translates positions through the means of rotational motion. To convert the rotational motion of the ball screw into a linear motion, a linear motion guidance must be implemented. Although conventional ball screws model does offer the choice that it comes with a default linear guidance, a concern regarding the load acting on the ball screw due to the length of the axis is raised. Hence, it is beneficial for us to design a motion guidance system for the ball-screw, with the capability to withstand and distribute the load from the ball screw. *Error! Reference source not found.* is the tally matrix constructed for evaluate the choices researched. Indirect stakeholder's concerns on the system are addressed via the efficiency of the guide system, where power loss due to motion of the guidance system ultimately creates more power loss on the long run. Safety measures are a mandatory measure when deciding for each sub-system.



Figure 4.2.4 - 1: Example V-Slot with Gantry Plate. [\[online\]](#)

The V-slot is the optimal choice for the application of ball screws. It triumphs due to the simplicity of the configuration, which results in a low effort to maintain and easy integration with other guide systems if needed. It can also withstand a high load, where the ball screw is heavier than other drive systems listed in the options. Roller tracks was a contending choice; however, it fell short on weight. Where additional weight from the guide system may compromise structural integrity of the system. As shown *Error! Reference source not found.*, this setup will only take up 3 out of the 4 rails available on the V-slot. This suggests that the additional rail can be used for other part (one of the designs in section 4.1.3 uses this). The combinations of v-slot and rail is also very common on the market, meaning that it can be replaced very

easily.

Guide systems for linear motion						
Evaluation Criteria	V-slot Rail with Plate	Electromagnetic Levitation	Telescopic Slides	Ball Bushings	Plain Bushings	Roller Tracks
Power Loss due to Motion	4	5	3	4	0	3
Initial Cost	4	0	5	4	5	3
Total Weight	3	0	4	2	3	1
Integration with Additional Guide Systems	5	3	3	4	4	5
Life Expectancy of System	3	5	4	5	2	5
Safety in Compliance to Industry Standards	4	5	4	4	2	3
Versatility for Veneer Size	5	3	5	4	4	3
Load Capacity	5	5	0	3	2	5
TOTAL	33	26	28	30	22	28

Table 4.2-3: Tally Matrix with Options for Guide Systems for Linear.

For the much shorter second axis, it is not required to have an additional support from the linear guidance, hence a much simpler approach can be taken. The main consideration when deciding for the second axis is the weight. As it is stacking on top of the longer axis, the weight of the axis directly influences the load of the motor. Inspired by the product in the market (*Error! Reference source not found.*), having two side bars on the sides can help in guiding the ball screw while keeping the overall weight down. This setup can also fully utilise the extra holes on the BK10 & BF10 component, which are acting as the end caps for the ball screws, hence further reducing any excessive resource needed for the guidance.

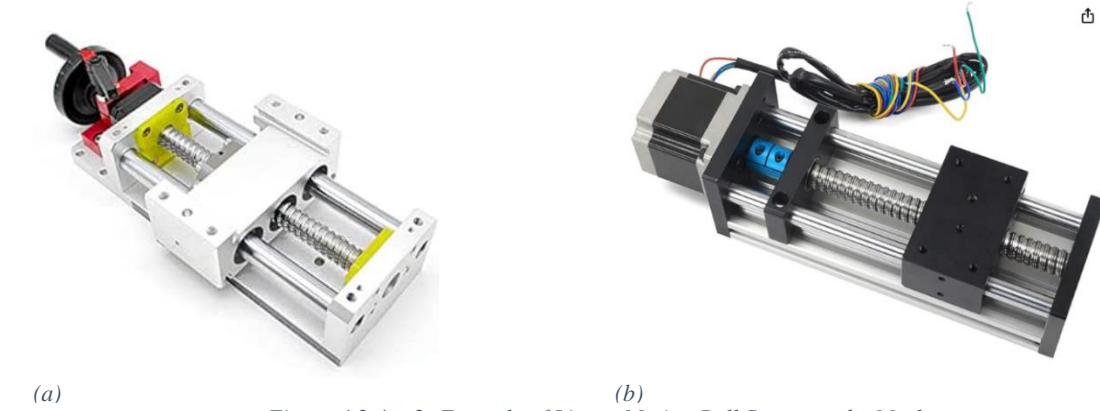


Figure 4.2.4 - 2: Example of Linear Motion Ball Screw on the Market.

4.2.5 Connectors

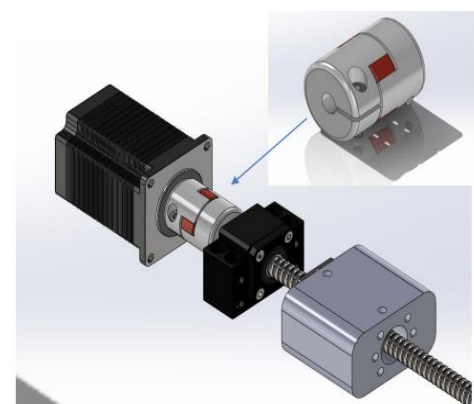


Figure 4.2.1: Demonstration of Beam Coupler.

The common method used in connecting the ball screw and a motor together are detailed in **Figure 4.2.5 - 2** with the optimal choice in this context goes to the beam coupler, under the category of shaft coupler due to the simple yet effective solution it provides. Unlike the gearbox or timing belt, it possesses no backlash, while possessing ease in installing and replacing, which is lacked by the direct coupling method. **Figure 4.2.5 - 1** illustrated the implement of a beam coupler in CAD. This configuration of the coupling between stepper and ball screw is hence applied on all 3 sets of them in

our system. To properly connect each sub-components together, some connectors need to be designed and implemented into the system. **Figure 4.2.5 - 3** illustrated the designed connectors when implemented into the CMM system. Component (a) and (d) holds the v-slots in place, while providing a base for the ball screw's component, BK10 and BF10 respectively for the primary axis in the CMM. Additionally, component (a) also acts as the housing for the stepper motor, thus also the connection of ball screw and stepper motor through the beam coupler lies on top.

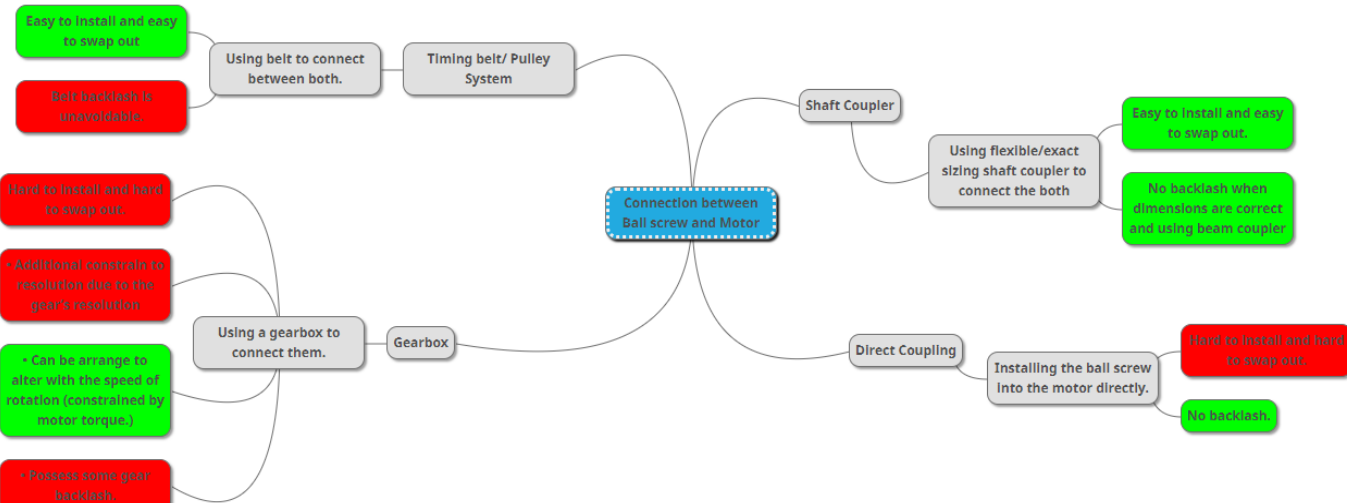


Figure 4.2-2: Mind map of method of connection between ball screw and motor.

Component (b) and (e) primarily connects to the ball screws' nut, in the meantime providing linkage between the ball-screw and the gantry plate. Furthermore, the secondary axis's ball-screw's BF10 and BK10 also lies on these two components, with another stepper motor and beam coupler specifically lies on component (b) only. Component (c) is designed to hold the Raspberry Pi HQ camera module, while still connects back to the ball screw's nut on the secondary axis. It is also crucial to have an extra two holes on the sides of this component (circled in red on component (c) in **Figure 4.2.5 - 3**), to fit in the two rods which will be acting as linear motion guidance specifically for the secondary axis, as discussed in **Section 4.2.4**.

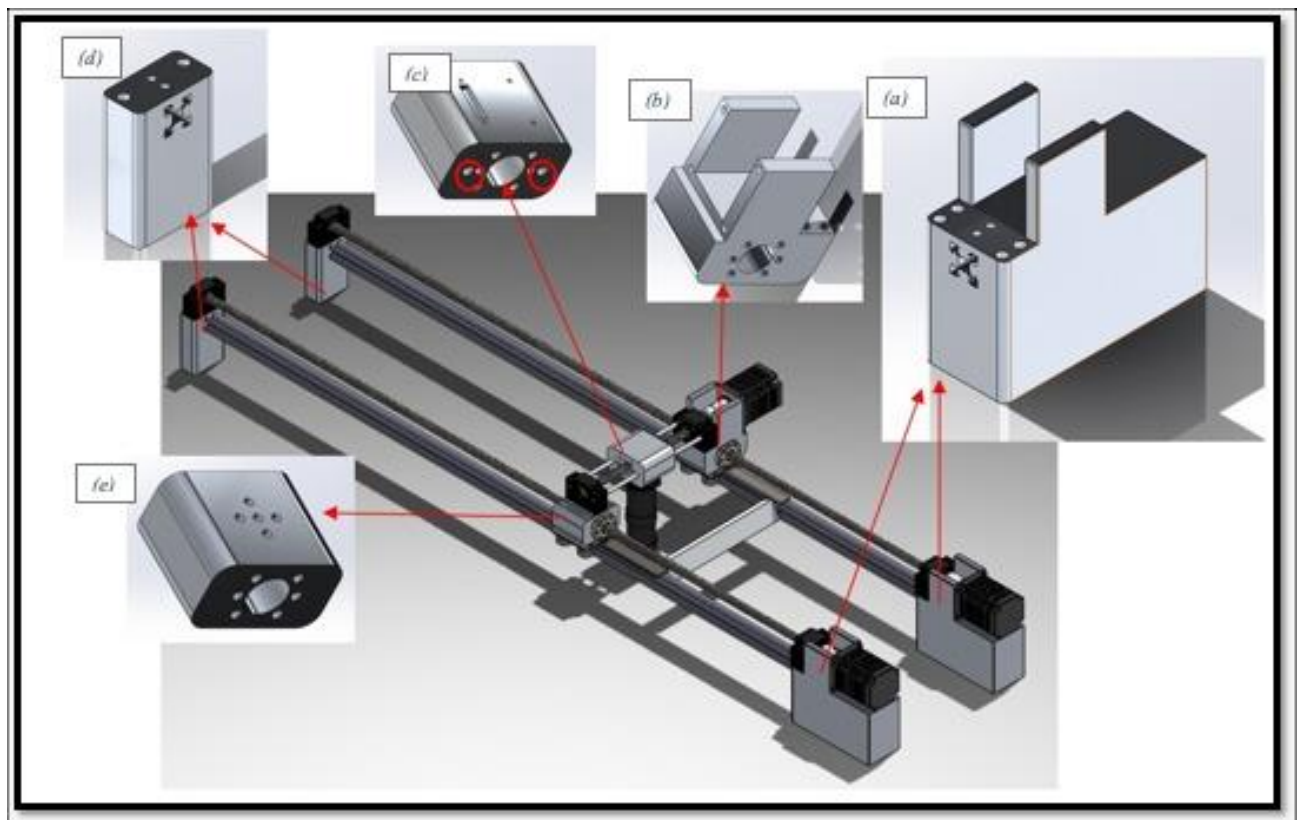


Figure 4.2.3: CAD Model of the CMM system including connector blocks and camera module.

The connectors designed in this section should all be manufactured using AA6061 aluminium alloy. As it is cheaper when compared to pure aluminium and lighter compared to steel. With ultimate tensile strength of 209 – 224MPa [22], it is providing sufficient strength to withstand the weight of the components (**Table 4.2.3 - 3**).

4.2.6 Aim and Objectives Covered.

The assembled sub-system to create the Gantry CMM with a camera satisfied the following aims and objective are:

Aims and Objectives Achieved	System Specifications
Veneer Size Coverage (Aim 2, Objective 1)	Projection maximum dimensions (950mm x 150mm), Smaller veneers can still be accessed with moving scanner module.
Environmental Considerations and Material Usage (Design Specification)	64% of total components used are recyclable
Safety (Design Specification)	From specifications, all sub-systems went through the safety criteria, purchasable components are ISO 12100 complaint.
Operating Conditions (Aim 5, Objective 1)	Machine can operate in atmospheric conditions, as most operating components are commonly found in the market.

Table 4.2-4: Aim and Objectives Covered.

4.3 Veneer Secure System

Wood veneer is prone to curling or warping due to minor temperature fluctuations or moisture exposure. This warping can compromise the consistency of data collected through camera imaging, as the primary stakeholder needs a system that can reliably detect areas of weakness. To ensure that the veneer remains flat for accurate imaging, a veneer stabilisation system is necessary.

Criteria	Clamp	Vacuum	Flat Plate	Frame
Safety (UK Machinery Safety Legislation)	2	5	5	2
Secure Veneer Attachment	5	5	0	5
Ensuring Flatness	5	4	0	5
Unobstructed View	0	5	5	0
Environmental Considerations and Material Usage (Cost)	3	2	5	3
Versatility in Size	0	5	5	0
TOTAL	15	26	20	15

Table 4.3-1: Tally Matrices of Options to hold Veneer still for Assessment.

Through meetings with the primary stakeholder, they specified that the largest veneer is 720mm by 125mm. The system should be able to capture a veneer as large as 720mm by 125mm as well as any sizes smaller than that. The safety requirements are a necessity to protect the operator during usage of the hardware, and environmental considerations

should always be considered to protect the environment, and lesser materials should be utilised to reduce the carbon footprint as well as the total cost expenditure.

The team's research indicates that it is essential to securely hold the veneer in place for the imaging system to function effectively. Any external movement can disrupt the image stitching software, leading to inconsistent and unreliable outputs. Furthermore, any physical obstructions can cause the software to generate inaccurate information about the obstructed areas. As previously mentioned, maintaining the veneer's flatness is crucial for producing consistent results.

Based on **Table 4.3-1**, it is evident that the vacuum system is the most favourable option, as it scored the highest total points. Which reflects its competence in meeting most criteria effectively. Although it does not perform as well as the clamp and frame in ensuring the flatness of the veneer, due to its reliance on suction rather than physical attachments, this is a minor shortfall when considering the overall advantages, the vacuum provides. Adding to that, the veneer is a delicate piece of thin wood, where a minimal amount of suction force will suffice in keeping it flat. The vacuum system excels at providing an unobstructed view of the veneer, where the clamp is not capable at due to its physical interference, while the frame creates glare due to its transparency. The clamp and frame methods have their specific advantages but, in this application, they are hindered with substantial drawbacks. Not to mention the safety concerns arising this configuration, where the clamp and frame may cause pinching of fingers of the operator.

The plain flat plate, while scoring second highest total points overall, exhibits significant restrictions in keeping the veneer secure and ensuring the veneer stays flat throughout the scanning process. This will affect the data consistency obtained via camera imaging. As a slightly warped veneer will cause inconsistencies in the grain length and any external forces can alter the position of the veneer outside of the maximum projected area of the camera. This undermines its practical utility despite its high score.

In summary, the vacuum system is the optimal choice due to its strengths in safety, coverage, view and versatility in size, combined with acceptable environmental and cost implications, making it the standout choice among the veneer support options presented.

4.3.1 Vacuum Tabletop

Taking inspirations from vacuum tables, a few preliminary designs were created. Such designs were purposed so that any issues or desired features with the selected design can be highlighted and pinpointed. Two surface types stood out, with conceptual proof of real-life counterparts. The first surface features a grid styled top (**Figure 4.3-1 . Grid Styled Vacuum Top**), which is inspired by wood making vacuum tables, shown in **Figure 4.3-2**.



Figure 4.3-1 . Grid Styled Vacuum Top

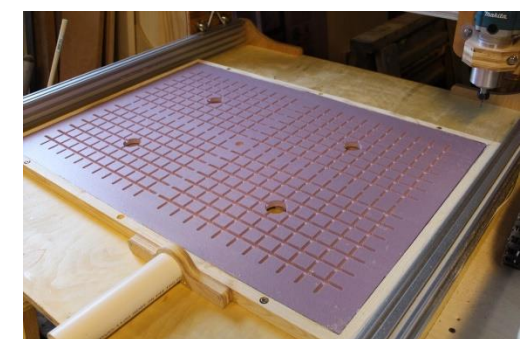


Figure 4.3-2 CNC Vacuum Table [23]

The grid style features suction holes and sunken pathways to distribute the suction. A rubber tube is to be utilised for this design to seal off the edges of the vacuum top. The rubber tube can be removable and can be reapplied depending on the veneer size. Its functionality has been proven with hard wood pieces, where the wood pieces must cover the suction holes to provide suction.

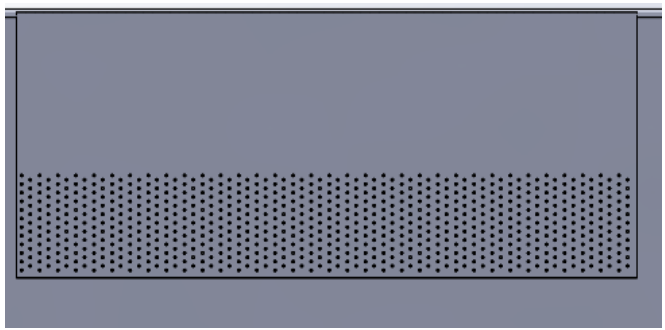


Figure 4.3-3. Grill Styled Vacuum Top

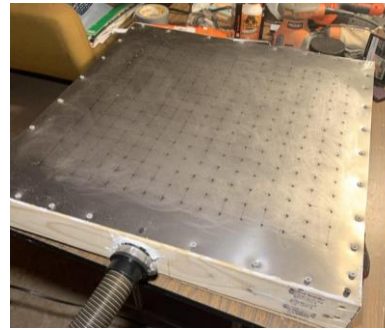


Figure 4.3-4. Vacuum Cloth Cutting Table [24]

In contrast, the grilled design provides suction by reducing pressure beneath the base. This design is more favourable because it is versatile with various veneer sizes and has demonstrated effectiveness in similar applications, such as cloth cutting. In these applications, the grill holes not covered by the veneer can be covered by a piece of plastic, enhancing its functionality. Additionally, the grill-style vacuum works by reducing the total pressure inside the chamber, making it effective even without the power of commercial vacuums.

On the other hand, the grid design, while proven to function with hardwood pieces, requires that the pieces must cover the suction holes to provide adequate suction. This design's large grids limit the dimensions of the veneer, reducing its versatility. Moreover, the grid-style vacuum top has only shown effectiveness with the power of commercial vacuums.

In summary, a grill styled vacuum top will be more appropriate for this application. However, both designs present with a manufacturing flaw. Where both designs integrate the tabletop into the base and are intended to be made from wood. However, machining wood for these purposes introduces unnecessary complexity. To address this, a separate steel plate can be used, shown below in *Figure* and *Figure*.

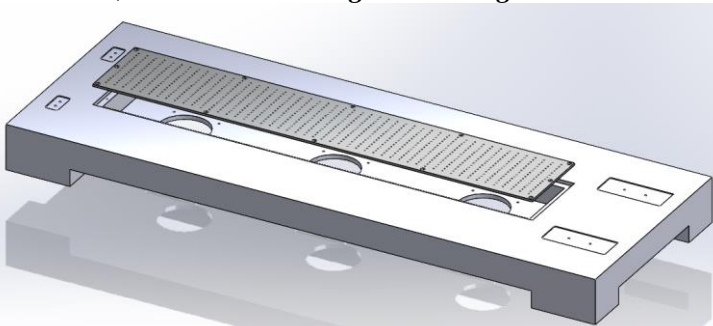


Figure 4.3-5. Vacuum table with exploded view of the steel grill plate top

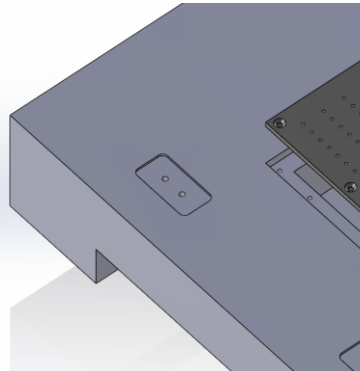


Figure 4.3-6 Steel Grill Plate top with ridges to show fitting

This plate attaches seamlessly to the base of the vacuum table using silicone glue for edge sealing to prevent any leakage of air and 12 CTSK Flat ISO 7046-1 M4 bolts to ensure the plate remains securely fastened.

4.3.2 Vacuum Chamber

Two methods for reducing pressure in the vacuum chamber were researched and incorporated into the preliminary design. The first method uses a tube connected to a motor to effectively lower the chamber's pressure, while the second method employs inverted fans to create a negative pressure differential from the surface. Shown below *Figure* and *Figure* respectively.

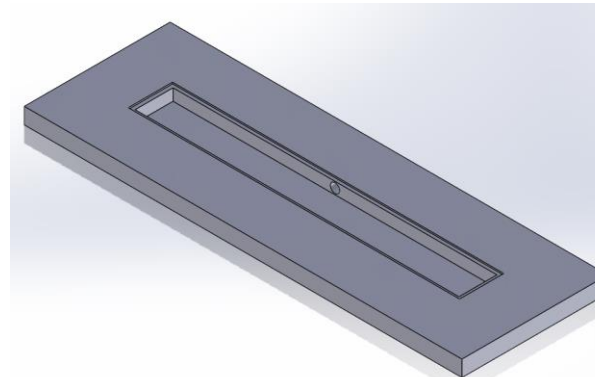


Figure 4.3-7. Chamber that features a connection to an external motor

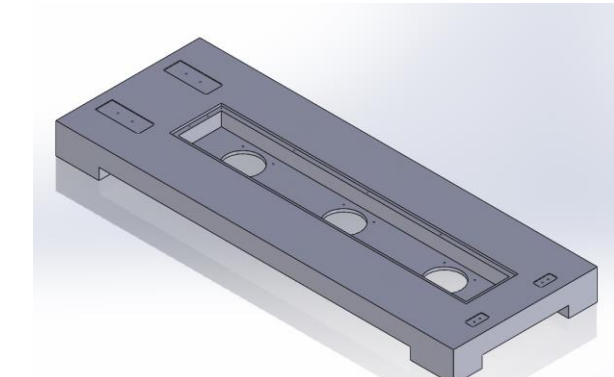


Figure 4.3-8. Chamber that features three holes, that are fitted with inverted fans to reduce pressure

Utilising Granta Edupack, the density and the coefficient friction of wood is obtained to be 600 kg/m^3 and 0.5 respectively. To calculate the pressure difference needed to provide a suction that will prevent the veneer from sliding, the friction force required to overcome sliding of the veneer must be calculated, which can be obtained from the force of the veneer from its weight multiplied by the coefficient of friction of sycamore wood. Utilising *Eqn. 4.3.2 - 1* and *Eqn. 4.3.2 - 2* respectively.

	$F_{\text{weight}} = \rho \times V \times 9.81$	<i>Eqn. 4.3.2 - 1</i>
	$F_{\text{slide}} = F_{\text{weight}} \times 0.5$	<i>Eqn. 4.3.2 - 2</i>

The pressure difference can then be calculated with the friction force required to overcome sliding of the veneer divided by the veneer area, shown in *Eqn. 4.3.2 - 3* as

$$\Delta P = F_{\text{slide}} / A. \quad \text{iEqn. 4.3.2 - 3}$$

The calculated pressure difference needed to prevent the veneer from sliding when secured on the vacuum system is 1471.5 Pa. Consequently, the use of a vacuum motor is deemed unnecessary. Additionally, overly strong suction could potentially tear the veneer. Vacuum motors not only create greater noise and consume more power, but they are also more expensive. Moreover, for the required low-pressure difference, the use of a vacuum motor is not necessary. Therefore, the design will proceed with the use of axial fans to provide suction for the veneer.

4.3.3 Fan Models

The pressure difference needed to generate suction for the veneer is very small, making ordinary axial fans used in PC cooling systems an excellent choice. 12V DC axial fans are readily available in the market, which is why they are selected for this purpose. Two common sizes are available: 80x80x25 mm and 60x60x25 mm fans. The larger 80x80x25 mm fans are chosen because they typically offer a higher airflow rate. Fan models from different brands, all with the same supply voltage and dimensions, are compared based on their airflow, power consumption, noise level, price and bearing type, shown below in *Table 4.3-2: Fan Models and their specification*

. A typical tally matrix is not utilised here due to the minute details that each fan bears, where tally matrices will be unable to justify in such manner as it is typically used to compare different types of models rather than variants of the same model.

Fan model	Airflow (m^3/h)	Power Consumption (W)	Noise Level (dB)	Bearing Type	Price £
RS Pro Axial Fan	68	2.9	34	Sleeve	10.34
ARX CeraDyna Series Axial Fan	67.5	2.88	34	CeraDyna A (Ceramic Bearing System)	10.81

Sunon EE Series Axial Fan	69.7	1.74	33	Ball	9.67
Sanyo Denki San Ace 9S Series Axial Fan	55.8	1.32	24	Ball	13.54

Table 4.3-2: Fan Models and their specification

From **Table 4.3-2: Fan Models and their specification**

, the Sanyo Denki San Ace 9S Series Axial Fan can be omitted as a contender of choices, despite the fan having the lowest power consumption and noise levels, it provides the lowest airflow at the highest prices.

The Sunon EE Series Axial Fan, highlighted in yellow is a standout option among the other fans due to several reasons. Firstly, the fitted ball bearings are advantageous over sleeve bearings, as it tends to last longer and is quieter at higher speeds due to ball bearings utilising a thicker lubricant which has a lower evaporation rate. Therefore, this omits the choice of the RS Pro Axial Fan, as it is equipped with the sleeve bearings at a higher price, noise level and power consumption.

However, one could argue that the ceramic bearing system is superior, as it is tested to surpass the durability of both sleeve and ball bearings. Additionally, they are resistant to static electricity and are less susceptible to heat buildup due to their poor conductivity of electric and heat. But the ARX CeraDyna Series Axial Fan, which is equipped with the ceramic bearing system, has the highest noise level, and second highest in power consumption and price. Adding to that, the airflow it provides in relation to the price and power consumption is not too efficient. In contrast to the Sunon EE Axial Fan, which has a similar noise level at 33dB. Provides $69.7 \text{ m}^3/\text{h}$ of airflow with a power consumption of 1.74 Watts, which has the highest airflow with the lowest price. Such trade-offs for additional longevity of the fan is not worthy, not to mention that ball bearing fans have a relatively long life. In conclusion, the Sunon EE Series Axial Fan is the choice of fan for its combination of high airflow, energy efficiency and acceptable longevity and noise levels.



Figure 4.3-9. SUNON Fan [10]

4.3.4 Veneer Alignment Tool

Initially, a simple sunken platform was used to align the veneer horizontally (**Figure**). However, this setup potentially affected the imaging system by creating shadows due to the lighting. To address this, a removable tab near the grilled surface was introduced to assist operators with the proper alignment of the veneer during insertion. Unfortunately, this introduced a gap in the base, which could potentially impact the HSV (Hue, Saturation, Value) colour parameters in the software. To resolve these issues, the removable tab was redesigned and relocated away from the camera's projection area (**Figure**).

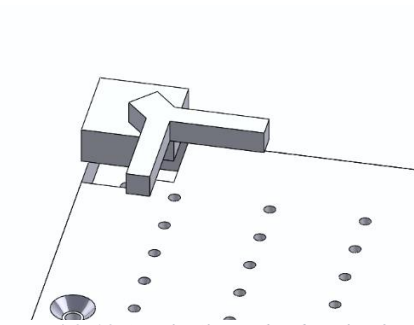


Figure 4.3-10 Simple Slot with L bracket for alignment, available on both sides of the plate.

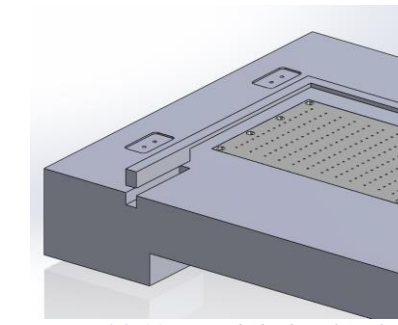


Figure 4.3-11. Extended L bracket along the length of the plate. With a slot further away from the plate to avoid camera projection

4.3.5 CAD (Vacuum Table)

The redesigned wooden table now features extended alignment bars and a slidable slot that integrates smoothly into the base. This design eliminates potential complications with the colour differentiation software, ensuring uninterrupted operation and no interference with the imaging system.

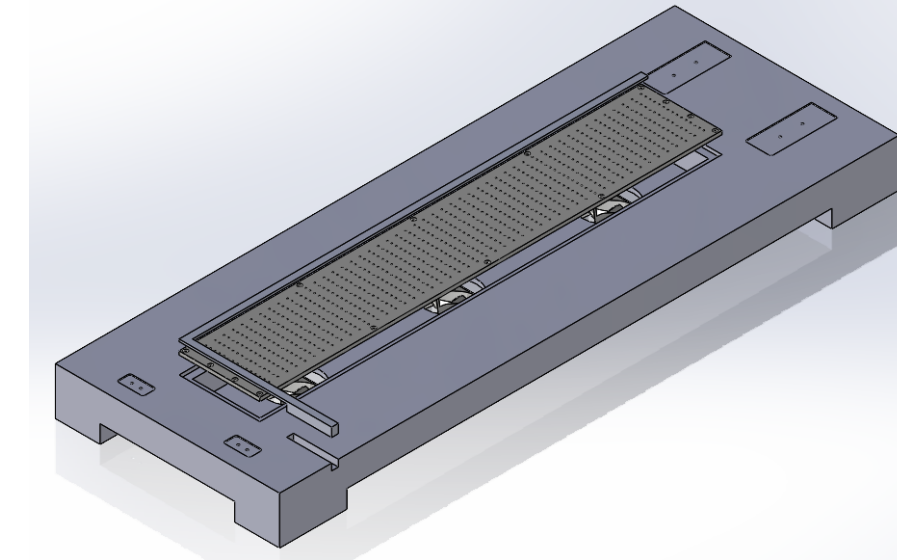


Figure 4.3-12. Isometric View of Vacuum CAD

The design specifications that the vacuum system satisfied are:

Aims and Objectives Achieved	System Specifications
Veneer Size Coverage (Objective 2)	Maximum veneer size that can be held flat (950mm x 150mm), Smaller veneers can still be held flat by covering the other holes that are not covered by the veneer.
Environmental Considerations and Material Usage (Design Specification)	Only axial fans are not recyclable, which by material surpasses the 60% requirement.
Safety (Design Specification)	Additional safety with the usage of low-speed axial fans as well as the noise levels being held below 70dB. Additions of diodes and fuse also protects the system and the user in any cases of voltage spikes.

Operating Conditions (Objective 2)	Vacuum system works in all conditions. Satisfies the atmospheric condition requirement
------------------------------------	--

4.4 Cake Tier Test Apparatus

The cake tier testing part is a tool that can be used to test the bending radius of wood veneer samples at varying radii, with the aim of finding stress concentrating features in the wood structure. The idea for this testing piece was found through research into bend testing schemes for the wood veneer to find areas of stress concentration, this method was used by Lunguleasa et al.[2] to find the critical bend radius of samples. Due to the similarity to the forming process to be used on the veneers in the project's context, the idea was developed to reflect the needs of the project as well as stakeholder requirements. This requirement was found through re-engagement with the stakeholder, who expressed an interest on the potential for this tool for identifying stress concentrations in new veneers as well as one that can be used in the field. This allows for assessment that they currently do not have to work with and therefore can achieve their requirement.

The value of this testing device would be in its ability to evaluate different wood samples to be able to assist the adaptability of the VENAS system, by being able to find stress concentration features in future veneers. This future proofing was a key requirement of the project as it allows the system to be used for any new veneers that the detection code is not currently tailored to. The attributes of the design are more focussed on specifics given by the stakeholders of the maximum bending radii that the wood veneer would need to sustain in the forming process. The maximum bending radius expected for the veneer was stated as 90 degrees and therefore a key attribute of the design is that it must be able to test bends of up to 90 degrees. Initial concepts were drawn up based on the test seen in the paper and split into two factors. These were decided to be the method of changing bend radius of the test and the method of applying the bend to the specimens. From these concepts the features were extracted and put into the tally matrices to assess the visibility of

Choice of Cake Tier test piece (varying dimensions)		
Criteria	Step design	Cone
Portability	5	5
Varying Diameter	4	3
User friendly	5	2
Manufacturing complexity	5	4
Imitate forming process	5	2
TOTAL	24	16

Table 4.4-1: Tally matrix for the varying dimensions of the bend

the different options against certain criteria. These criteria were chosen to reflect the specification and the intended purpose of the apparatus. These matrices can be seen in **Table 4.4-1** and **Table 4.4-2**.

In this matrix the features from concepts have been tally against the criteria outlined in the requirements of the apparatus. This matrix focusses on the load application part of the apparatus where the brackets would apply the bend to the material being tested. The scoring on this matrix came out in favour of the single piece bracket for applying the load. Its manufacturing complexity is a disadvantage of the design but the advantages in the other criteria outweigh this.

The next aspect of the design that was assessed using a matrix was the method of changing diameter or the bending radius. The two options proposed in the concepts was a cone design and the other a step design. This tally matrix is shown in **Table 4.4-1**.

The step design scored higher than the cone design, despite its restriction of varying diameters. This meant that it was the more favourable option for its intended purposes.

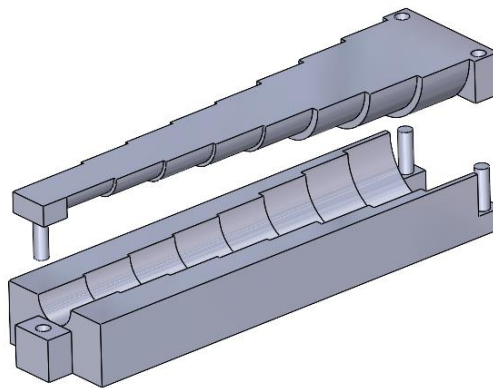
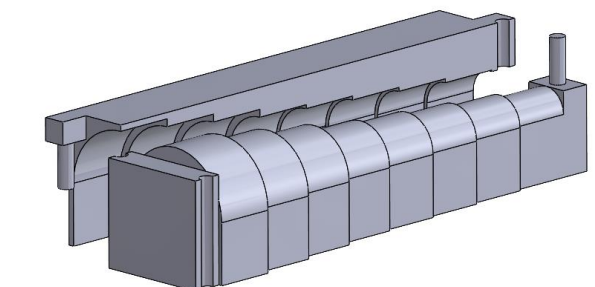


Figure 4.4-1: Iteration of Cake Tier apparatus design focussed on 180-degree bends.



These options were then pursued in CAD designs beginning with an early stage of the cake tier design that would be used in bend tests of the veneer, which used a step design, but the brackets were without backing and were separate pieces. This design was produced via 3D printing using ABS plastic and the main piece can be seen in Figure 3.2-1. Due to a lack of backing or a guidance method for the piece, it was not able to achieve the desired reliability alongside the bend itself. This design was developed to utilise a combined bracket design to improve the portability of the apparatus and locator pins added to improve the repeatability of the tests to be performed with it. This iteration of the design, Figure 4.4-1, included vertical locator pins that would considerably improve the repeatability of the tests and in turn, the apparatus' reliability.

Bend angle of 180 degrees can be performed reliably and repeatedly at varying radii with this iteration of the design but from stakeholder engagement, it was evident that the veneers were not expected to undergo bend of this angle. While it could be said that if the veneer could undergo a 180-degree bend without failure, it would also be able to withstand a 90-degree bend as well. It was decided that the design should be modified to focus on achieving the 90-degree bend but also be able to complete a larger angle bend if necessary.

This design has been modified in both the application of the bend as well as the locator pins. In terms of the bend application, this now occurs from the side in this configuration with an extended flat plate from the curved surface. The benefit of this is that it allows the 90-degree bend to be performed while keeping the samples aligned. The locator pins have also been altered to allow for the sideways motion to apply the bend while still maintaining its purpose of improved repeatability, however, this configuration would not allow for continuous guidance through the whole application of bend. This design option was therefore altered to use a system of removable locator pins, that would allow for both continuous guidance but also achieve this for both the 90-degree bend and the 180-degree bend configuration. This design

Choice of Cake Tier test piece (load application)					
Criteria	Hinged bracket	Separate brackets (no backing)	Separate brackets (with backing)	Single piece bracket	Hand bending
Portability	4	0	0	5	5
Varying Diameter	5	5	5	5	5
User friendly	1	1	2	5	3
Manufacturing Complexity	2	4	1	0	1
Imitate forming process	3	2	4	5	2
TOTAL	15	12	12	20	16

Table 4.4-2: Tally Matrix for load application options

can be seen in Figure 4.4-3, which shows how the locator pins are used for both alignment of the top part as well as connection of the two top halves when performing 180-degree bends, seen in Figure 4.4-4.

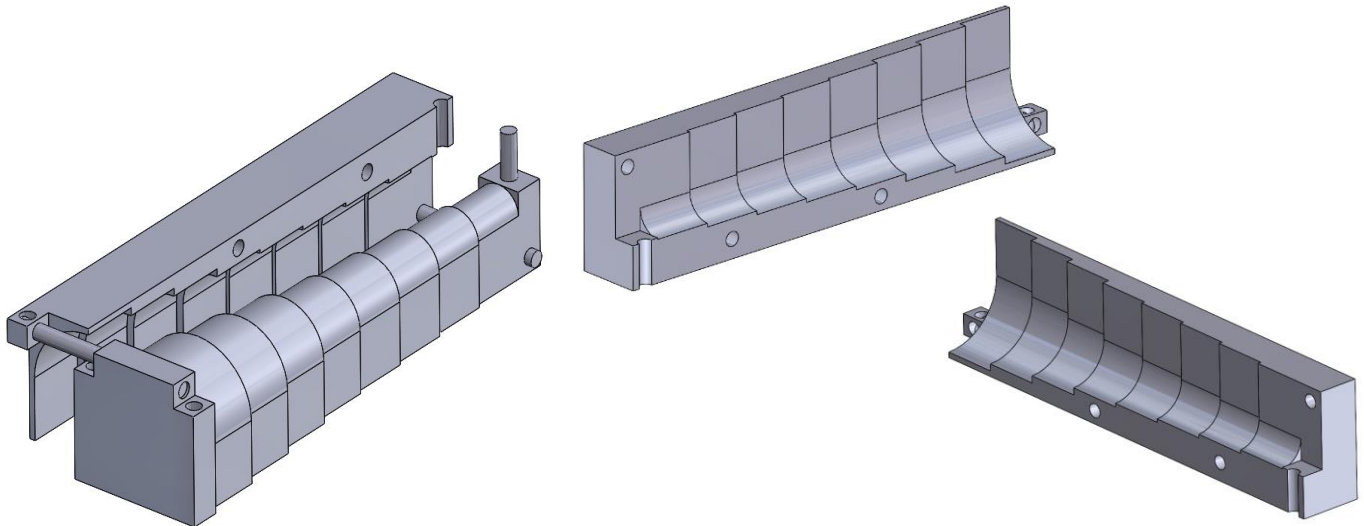


Figure 4.4-4: Left: CT design with updated locator pins (90-degree configuration), right: two halves of the top bracket used to apply bend.

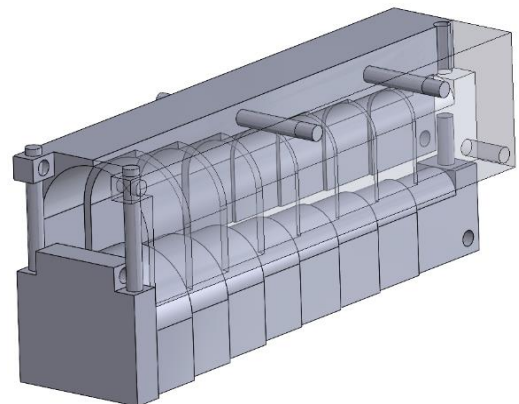


Figure 4.4-3: Left cake tier design (180-degree configuration), right:

Choice of Cake Tier test piece (material)			
Criteria	Plastic (abs)	Aluminium	Stainless Steel
Sustainability	1	4	3
Manufacturing difficulty	3	3	3
Surface finish	3	4	2
Weight of part	5	4	1
TOTAL	12	15	9

Figure 4.4-2:Tally matrix for material selection.

For the material selection of the apparatus, three options were considered. These were ABS plastic, cast stainless steel and cast aluminium, which were chosen due to the availability and low costs. These materials were compared using a tally matrix, Figure 4.4-5, which judged the options based on the sustainability of the material use, manufacturing difficulty, surface finish and weight of the part. These were chosen for varying reasons but focussed on the impact of the piece and its usability in the field, a desire of the stakeholder found during re-engagement. Surface finish was assessed based on the machinability of each material type was an important consideration as a rough surface could impact the reliability of the bend tests, through load concentrating features. The sustainability of the material use for each part was

compared using data for the energy usage and the carbon footprint for the material, manufacture and the end of life using Granta Edupack.

Aluminium has scored the highest from this matrix due to its high recyclability, high machinability as well as low density and thus low weight of the part. It should be noted that ABS, which was the material used to 3D print the initial cake tier test piece, has benefits of a lower weight and similar surface finish and manufacturing difficulty but due to a poorer sustainability score, it cannot be recommended. The piece should therefore be manufactured using AA6061 recycled aluminium alloy, which is a recyclable material which boasts environmental considerations. The cake tier apparatus achieved the following aims and objectives with its specification:

Aims and Objectives Achieved	System Specifications
Portability (Objective 3, Aim 1)	Apparatus is 0.87kg if manufactured with aluminium and therefore below the 1.4kg weight threshold for handheld devices
Environmental Considerations and Material Usage (Design Specification)	Entire piece is made of AA6061 recyclable aluminium alloy, which is readily recyclable.
Varying Diameter	The apparatus curves have varying diameters from 40mm at the largest tier, based on the calculated critical radii of this veneer, to 15mm at the smallest tie.
Operating Conditions (Objectives 5, Aim 1)	Apparatus works in all conditions. Satisfies the atmospheric condition requirement.
Imitate Forming Process (Design Specification)	Cake Tier imitates forming process by varying radii in each tier.
User Considerations (Design Specification)	Relatively simple configuration, that is easy to use.
Safety (Design Specification)	Bend are applied manually using bracket, injuries that are caused by clamping of the two Cake Tier pieces are minor.

Table 4.4-6. Aims and Objectives Achieved.

5 Operating System

The system requires a small single-board computer (SBC) for post-processing captured images, and the Raspberry Pi fits well within the budget constraints. Additionally, the Raspberry Pi ecosystem is robust, with a wide variety of components readily available online. Consequently, the Raspberry Pi was selected. Table 4.4-1 below shows a comparison of two Raspberry Pi computer boards that were considered for this purpose. Raspberry Pi 4 and 5.

Board Model	Raspberry Pi 4	Raspberry Pi 5	Comparison
CPU	Quad core Cortex-A72 (ARM v8) 64-bit @ 1.8 GHz	Quad-Core Cortex-A76 (ARM v8) 64-bit @ 2.4 GHz	2-3x performance on Pi 5
RAM	1,2,4,8 GB	1,2,4,8 GB	
Price	£72	£76.80	Pi 5 more expensive by £4.8
OS and storage	Micro SD	Micro SD with support for high-speed SD104 mode	2x interface speed on Pi 5
Real-time clock (RTC)	n/a	RTC and RTC battery connector	Pi 5 has RTC

Table 4.4-1. Comparison of performance, Pi 5 and Pi 4

On paper, the Raspberry Pi 5 will be more feasible due to the better performance and highest interface speed provided, as well as having a real-time clock. Which may be useful for any future updates on the Pi 5 that may require it. It is more expensive than the Pi 4, however the price difference is marginal for the benefits it provides for this application. Adding to that, the thermals of the Raspberry Pi 5 is lower than the Raspberry Pi 4 at full CPU load, shown below in Figure and Figure , respectively. It is noted that the Raspberry Pi 5 will have a relatively better performance than the Raspberry Pi 4 under full CPU load due to their respective specifications. A cooler fan is added to the Raspberry Pi 5, to increase the longevity of the single board computer as well as maximise the efficiency of the Raspberry Pi 5 during high workloads and queues.

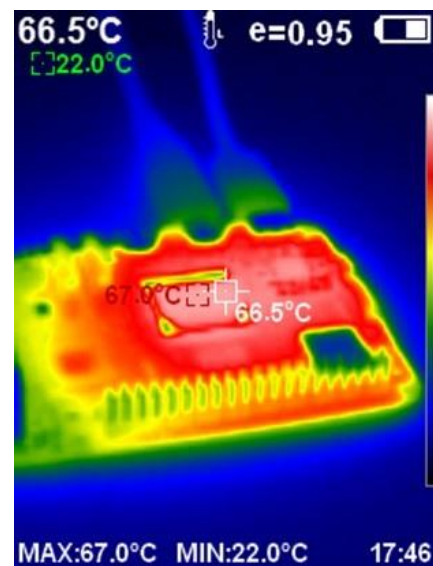


Figure 4.4-1. Raspberry Pi 5 thermal image [25].

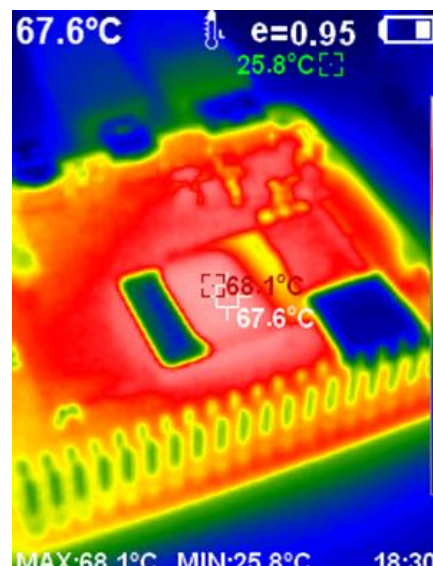


Figure 4.4-2 Raspberry Pi 4 thermal image [25].

6 Electronics

6.1 Circuit Diagram

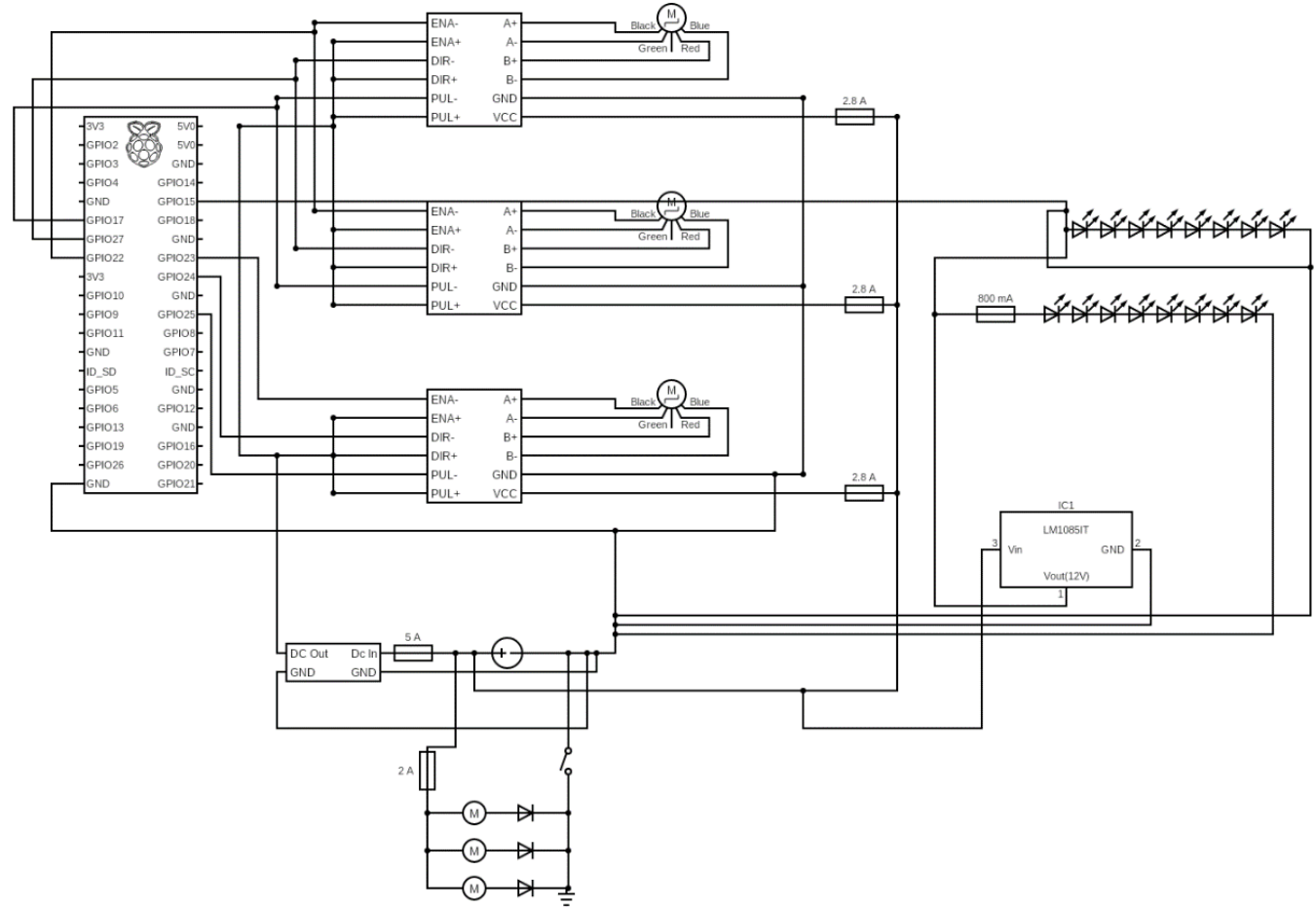


Figure 6.1 - 1: Overall Circuit Diagram for the System.

The circuit primarily consists of a Raspberry Pi 5, motor drivers, stepper motors, and Ultra LED light strips. The motor drivers are connected to the Raspberry Pi using a PNP setup, where the positive outputs are linked to the control inputs. This connection is favoured for its familiarity among technicians, facilitating easier operation by stakeholders. It is advised against connecting the ENA/DIR/PUL + ports directly to the Raspberry Pi's 5V output; instead, these are connected to a 3.3V DC-DC converter protected by a 5A fuse, powered by a DC supply. The negative signal ports return to the Raspberry Pi's signal ports on the GPIO, with two drivers sharing the same GPIO in a series setup, to ensure the simultaneous movement between them.

Each driver's ground and voltage input link back to the power source, safeguarded by a 2.8A fuse, with a parallel setup among the three drivers for consistent voltage. The Ultra LED light strips are connected to a 12V constant voltage regulator, ensuring uniform brightness, and protected by an 800mA fuse. The WS2815B light strips, featuring 4 pins, connect the voltage in pin parallel to the Ultra LED to the 12V regulator. The ground (GND) and backup input (BI) pins connect to the universal ground, while the data input (DI) pin links to a GPIO pin on the Raspberry Pi. For these light strips, only the first LED requires connection; for subsequent LEDs, the BI pins are pre-connected to the preceding DI pins to prevent control loss from a single faulty DI pin.

As mentioned on paragraph above, the stepper motor requires a logic driver for it to be functioning. The only restriction in selecting the driver would be a continuous 2.8A of current required by the NEMA 23 (23HE30-240S), and the

compatibility of the driver towards a stepper motor. After the process of selecting and eliminating, with choices illustrated in *Figure 6.1 - 2*, the optimal choice in this context, will be the TB6600 stepper motor driver.

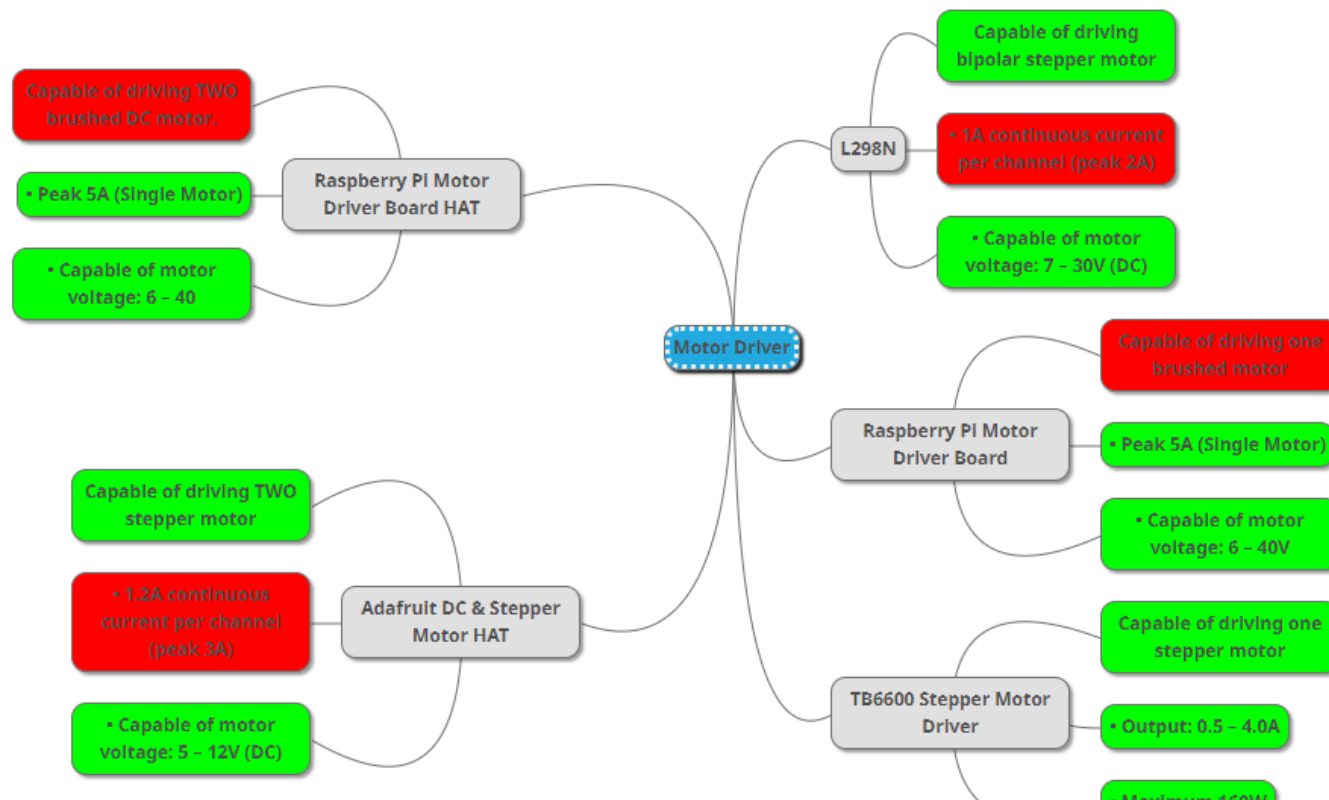
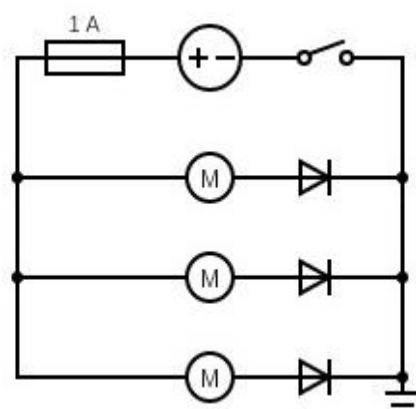


Figure 6.1 - 2: Mind map of the Motor Driver.

A simple 12V DC power supply can support three fans in parallel, shown in *Figure 6.1 - 3*. The fans are symbolised by the motors in the diagram. A 1A fuse is utilised in series with the power supply which serves as overcurrent protection. Which protects the components from damage from excessive current. Extra safety measures include diodes for each motor in parallel. This is to protect against voltage spikes caused by inductive kickback when the motors are switched off. This will prevent damage to other sensitive components in the circuit, as this circuit will be integrated into the overall circuit of the system. The inclusion of a switch aids in manual control of the motors, where the motors can be turned on manually once the veneers are well positioned. This also allows the circuit to be manually disconnected if required. The circuit is also grounded to prevent any build-up of voltages that might damage the components or hurt the user, it also acts as a return path for current and reference point for voltages within the circuit.

Figure 6.1 - 3: Circuit diagram of vacuum system.



7 Software

7.1 Model Selection

The selection criteria for a machine learning model tasked with identifying stress concentration-causing features using camera vision are as follows:

- Achieve a detection accuracy greater than 68%, in line with stakeholder expectations.
- Ease of use, requiring no additional configuration after initial setup for specific veneer types and setups.
- Compatibility with Python, ensuring seamless integration with most open-source operating systems, even on modest computing platforms.

Classical feature detection models	Deep learning approach
Support Vector Machine (SVM)[26]	Convolutional neural networks (CNN)[6]
k-Nearest Neighbor (KNN)[26]	N/A
Mahalanobis distance[27]	N/A

Table 7.1-1: Techniques that have been applied to identify features on wood surfaces.

Table 7.1-1: Techniques that have been applied to identify features on wood surfaces.

provides a comprehensive overview of the methods used to recognise wood surface features in various literature sources. Traditional detection models rely heavily on feature engineering techniques such as principal component analysis (PCA) to function effectively. This reliance is due to the inherent limitations of classical models, which tend to ignore spatial relationships and feature learning at multiple levels of abstraction.

In contrast, deep learning methods, particularly those utilising convolutional neural networks (CNNs), can transcend these limitations and potentially achieve higher accuracy rates. However, they require longer training times and larger datasets. As observed by Pin Wang, Fan En and Peng Wang [28], classical methods tend to outperform CNNs when run on smaller training datasets, typically comprising around 800 samples. However, as the dataset size increases beyond approximately 7,500 samples, CNNs become the superior model, demonstrating their scalability and effectiveness when dealing with large datasets.

However, given the dense and relatively small features inherent in the veneer within this project, employing convolutional neural networks (CNNs) would prove prohibitively expensive and unlikely to yield high accuracy, as corroborated by the prototype outlined in the subsequent section, Section 7.1.1. In addition, the classical model presented in the literature relies heavily on the feature reduction algorithms to work, which are specific to different wood types. Consequently, there arises a need to develop a model that does not require extensive data pre-processing and instead leverages simple camera vision algorithms to identify problematic features.

7.1.1 Prototype of CNN



Figure 7.1-1: A comparison between the (a) True label and (b) the label by the CNN model.

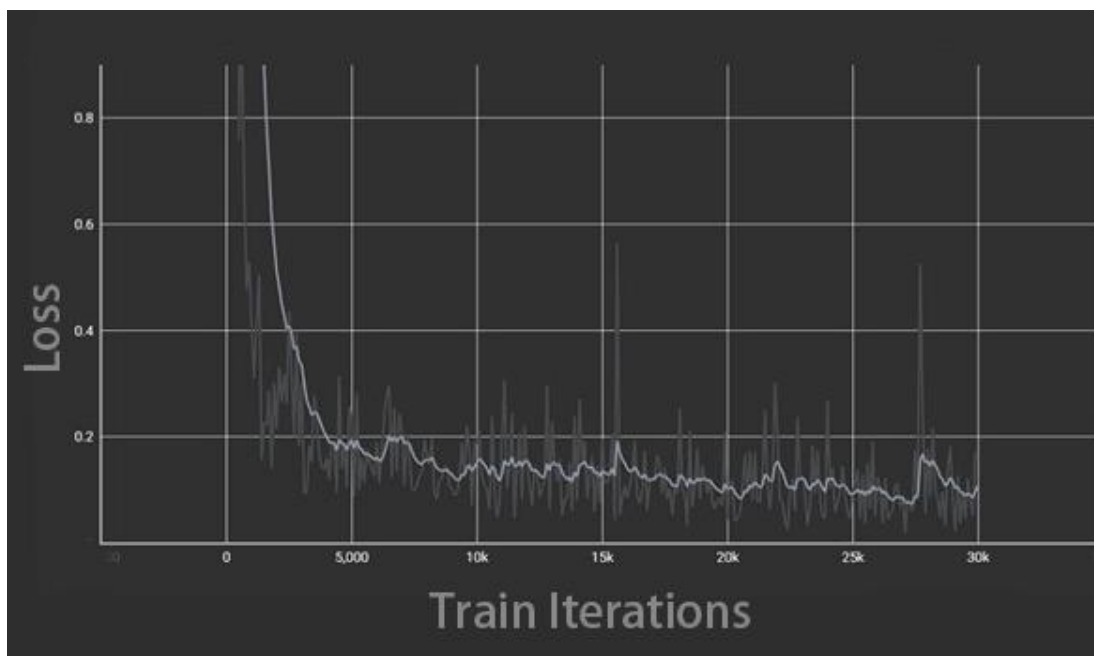


Figure 7.1-2: Training loss of the CNN model over iterations with the lighter curve showing the actual raw data and the darker curve showing the smoothened curve.

To ascertain the viability of employing convolutional neural networks (CNNs) within this project, a CNN model was developed to detect large knots and strikes on wood surfaces. The loss is a function that compares the target and predicted output, indicating how well the neural network models the training data. The results of the training, conducted with eight samples and validated with two samples, are depicted in Figure 7.1-1: A comparison between the (a) True label and (b) the label by the CNN model., while the corresponding loss of the model is illustrated in *Figure 7.1-2*.

Figure 1 reveals that the model successfully identifies larger and more prominent features but struggles with smaller ones. This limitation is evident from the jagged fluctuations observed in the loss function depicted in Figure 2, which are attributed to the relatively small sample size used for training. Consequently, the CNN model appears unsuitable for the project's objectives.

This conclusion is further reinforced by the characteristics of the veneer provided by stakeholders, which are typically small and dense. Furthermore, the time-consuming process of annotating all relevant features for training further detracts from the practicality of using CNNs in this context.

7.2 Feature Detection Algorithm

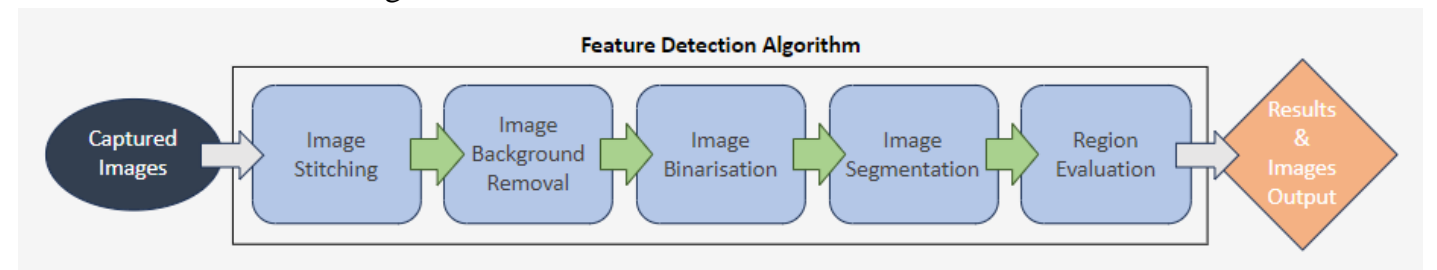


Figure 7.2-1: Feature Detection Algorithm Flowchart

The focus now shifts towards the development of a feature detection algorithm independent of machine learning methodologies. This strategic decision was motivated from various considerations including the challenges faced by CNN models in accurately capturing smaller and denser features present in the provided veneer samples. Additionally, the time-consuming nature of large-scale data collection and the resource-intensive task of annotating training data for machine learning algorithms further influenced the decision. Furthermore, the feature detection algorithm's ability to operate with computational efficiency, without necessitating top-of-the-line computational components, was a significant consideration.

Illustrated in Figure 7.2-1 is the feature detection algorithm flowchart, comprising five main sections: image stitching, image background removal, image binarization, image segmentation, and region evaluation.

7.2.1 Image Stitching

Stitching Algorithms		
Criteria	Based on Motor Movement	Based on pixel movement vectors
Development Simplicity	2	2
Effort in Maintenance	2	5
Computing Power Requirement	3	2
Cost Based on Hardware Requirement	5	5
Stability	1	3
TOTAL	13	17

Table 7.2-1: Tally matrix for different stitching algorithms.

To enable the implementation of feature detection algorithms on captured images, it is imperative to use an image stitching methodology to process images acquired individually by the camera. **Table 7.2.1-1** shows the tally matrix comparing different stitching algorithms considered in the initial design stage. The proposed technique of using overlapped features by Webel et al. [29] is adopted, which differs from conventional stitching methods used in microscopes and smartphones that rely on movement sensors to aid in alignment. This method allows for image stitching without requiring movement information, which significantly reduces the dependence between the movement system and the software. As a result, it simplifies maintenance and development processes, providing a more efficient and streamlined solution.

7.2.2 Image Complexity Reduction (Binarisation)

The decision to simplify image complexity stemmed from stakeholder feedback and insights gleaned from prior studies. These insights suggest that defects likely reside along the border between the lighter and darker rays observed on the wood veneer surface. Although later structure analysis results indicated that the features indicating weak regions come from the white speckles on the wood veneer surface, the binarisation of the images would similarly enhance the detection of these critical features, while simplifying the image for subsequent analysis.

Initially, an image binarisation approach using Euclidean distance was devised. However, testing revealed significant inconsistency in the binarisation process. To address this, an alternative method employing grayscale thresholding was explored. Grayscale thresholding involves grayscaling the wood veneer image and setting a threshold value within the

8-bit grayscale range. Pixels with values larger than the threshold turn white, while those smaller turn black, effectively binarising the image.

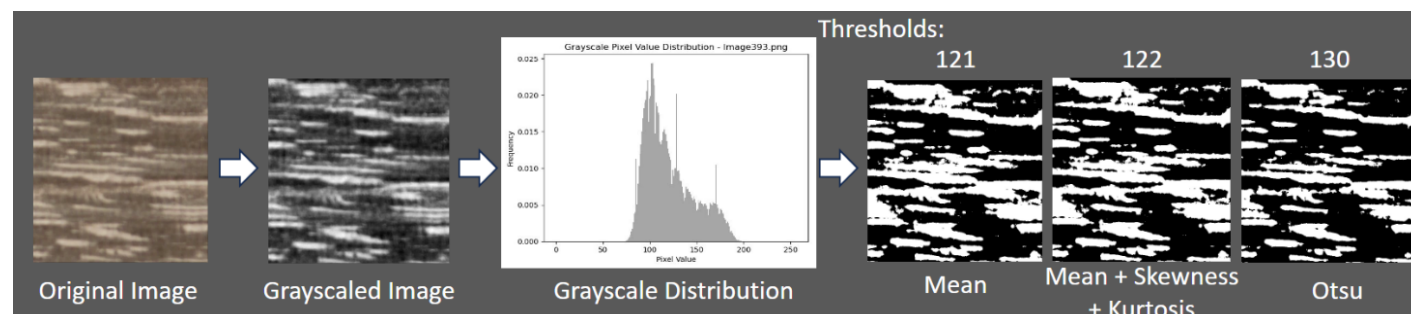


Table 7.2-2: Binarisation of an image of wood veneer surface utilising grayscale thresholding with 3 different threshold approaches

The initial threshold value was determined using the mean of the grayscale distribution of the grayscaled image. While this method showed some improvement in consistency compared to the previous approach, it did not properly binarise the image, converting some darker regions to white instead. Further analysis of the grayscale distribution revealed skewness and kurtosis. Incorporating these values into the threshold calculation provided some enhancement; however, it still fell short of capturing all pertinent information.

Ultimately, Otsu's method, developed by Nobuyuki Otsu [30] was selected for binarisation due to its effectiveness. By iteratively searching for the optimal threshold that maximises inter-class variance, this method consistently and reliably binarised the images. However, testing uncovered challenges with images under poor lighting conditions or containing irrelevant backgrounds, resulting in suboptimal binarisation results. These challenges were addressed in the design process and in the subsequent section.

Subsequently, image binarisation effectively reduces the complexity of the image, which for the specific wood veneer provided by the primary stakeholder, works well as the important detected feature is aided by the simplifying nature of binarisation. However, for other types of wood veneer, where important features may lie in the more complex layers of the wood veneer surface, binarisation would potentially remove these features entirely.

7.2.3 Image Background Removal

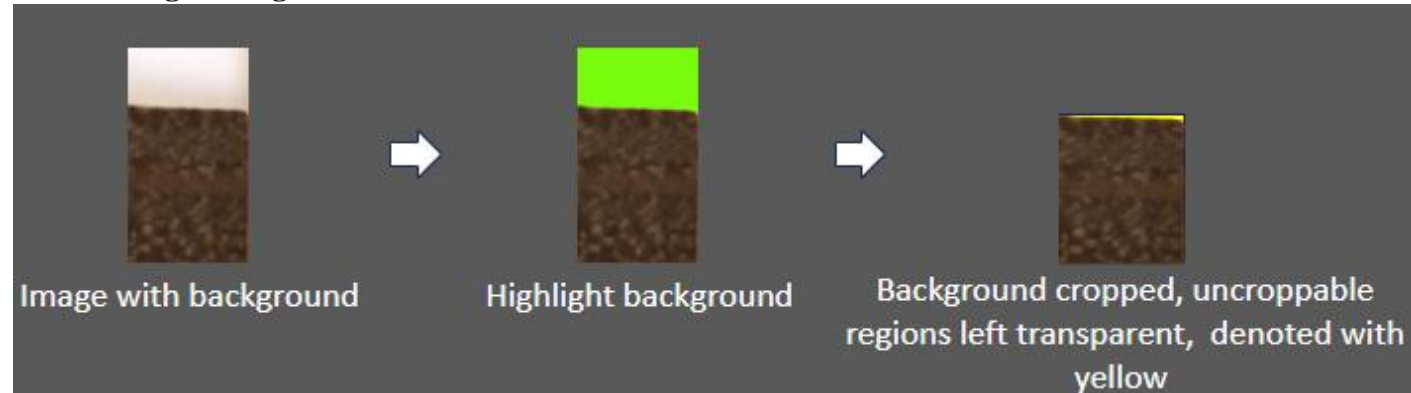


Figure 7.2-2: Image Background Removal Process.

To address the challenges encountered by the image binarisation process, an image background removal algorithm was developed. Figure 7.2.3-1 illustrates the image background removal process. It's notable that the algorithm attempts to crop out the background. However, for wood veneer images captured without entirely straight edges, complete removal of the background may not be achievable. Instead, the background is cropped until the furthest point where the wood veneer may lie, and the remaining backgrounds are left as transparent. This limitation arises from the necessity for the image to maintain a quadrilateral shape.

Although this drawback would not affect the subsequent evaluation process of the veneer surface, it would impact the image segmentation process. Regions with these transparent pixels would show less overall wood veneer surface compared to other segmented regions. However, the vacuum system addresses this drawback through the inclusion of a veneer alignment tool. This tool ensures that for quadrilateral wood veneers, such issues would not arise.

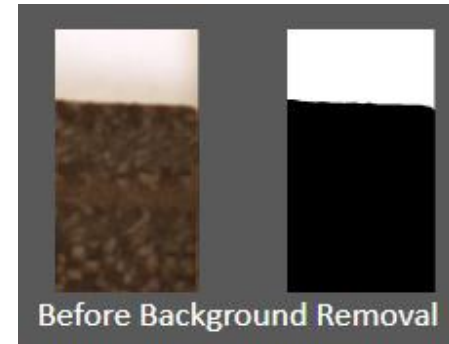


Figure 7.2-3: Binarisation of an image of wood veneer surface containing irrelevant background



Figure 7.2-4: Binarisation of an image of wood veneer surface after background removal.

As evidenced in Figures 7.2.3-2 and 7.2.3-3, the influence of the background during the binarisation process is notable. Prior to background removal, the features within the wood veneer are not discernible post-binariation. However, after undergoing background removal, these features become distinctly visible.

It is worth noting that the binarisation process does not consider transparent regions. Consequently, for images containing transparent areas, only the wood veneer surface is considered during binarisation.

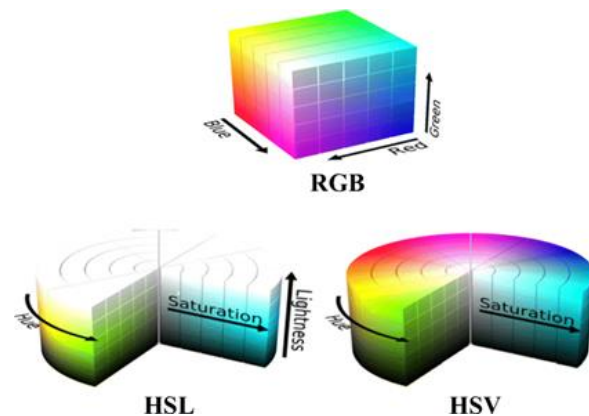


Figure 7.2-5: RGB, HSL, and HSV colour coordinates [software ref.no. 1.]

7.2.3.1 Wood Veneer Colour Investigation

To pinpoint the range of colour values that do not correspond to the wood veneer, a series of wood veneer images were captured using the prototype system under the prescribed lighting setup. These images were then subjected to a colour investigation algorithm. This algorithm compiled and plotted the distribution of pixel colour values specific to the wood veneer across the images. Through this process, the range of colour values that deviate from the wood veneer's characteristics could be accurately identified.

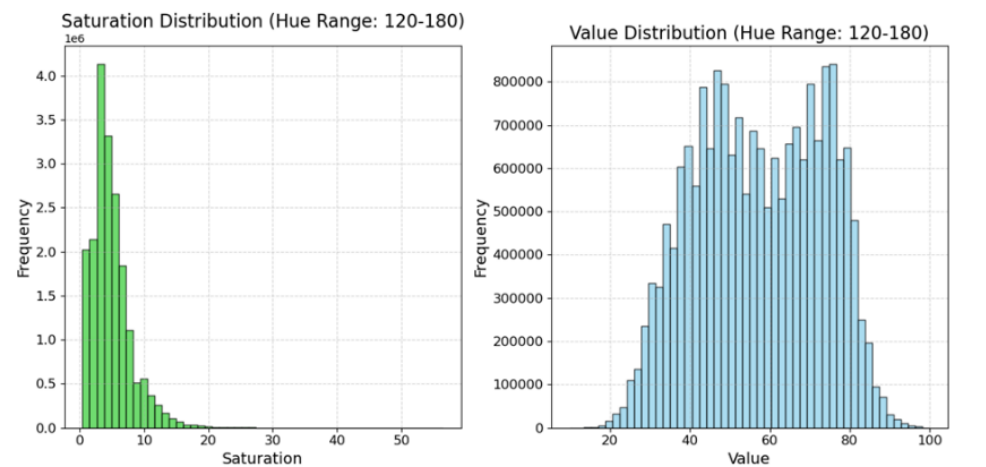


Figure 7.2-6: HSV Colour Investigation Colour Distribution (Hues 120 – 180)

The colour investigation algorithm systematically analysed the HSV colour coordinates across hues ranging from 0° to 360° , at intervals of 60° , ensuring a thorough examination of the colour spectrum. Subsequently, the saturation and value within each interval were examined, identifying hues between 120° and 180° exhibited the narrowest range of saturation, spanning from 0% to 57%. Conversely, the value distribution across all intervals encompassed the full range from 0% to 100%. These findings, illustrated in Figure 6.2.3.1-1, suggest that the background colour should ideally fall within the hue range of 120° to 180° , with saturations exceeding 57%. Therefore, it was determined that the background of the imaging system would consist of colours with HSV values of hue of 142° , saturation of 80%, and value of 69.8%, illustrated in Figure 7.2.3.1-2, accommodating potential variation in colour due to factors such as lighting conditions and imaging inaccuracies.

While this process efficiently removes the background from images captured by the final system prototype, it is important to note that it is most suitable in removing backgrounds for the primary stakeholder specified wood veneer, as other wood veneers may lie within the excluded range of colour values.

7.2.4 Image Segmentation: Grid-based Region Splitting

To address the primary stakeholder's concerns about identifying regions to avoid on a piece of wood veneer during manufacturing, segmenting the wood veneer surface image would enable region-based evaluation, effectively addressing these concerns.

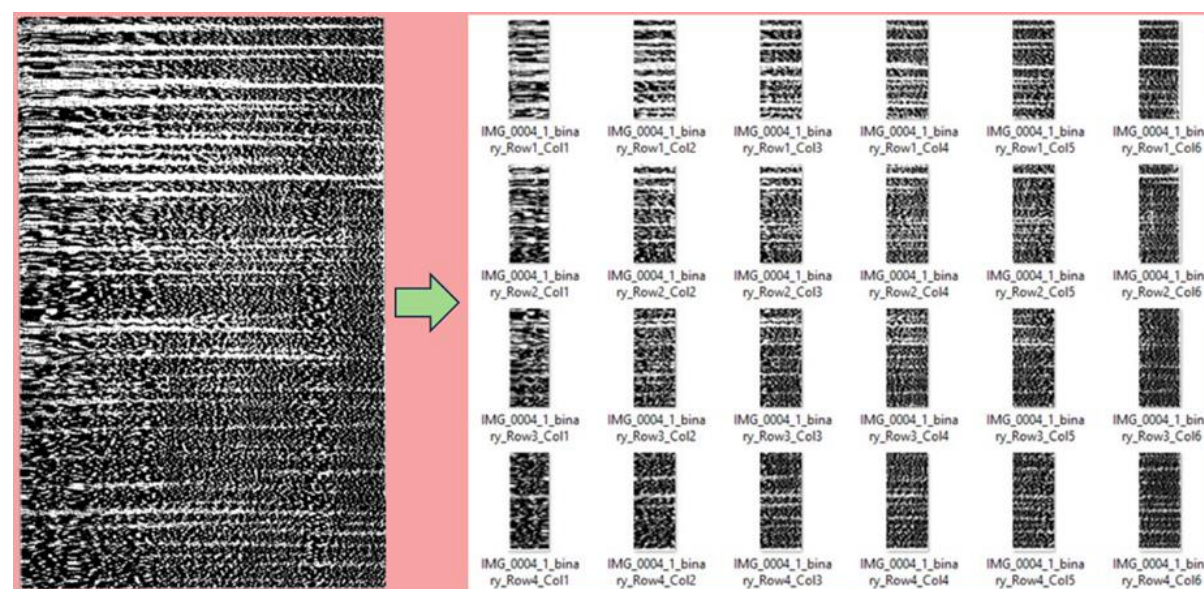


Figure 7.2-8: Image segmentation of a binarised wood veneer surface (4 rows, 6 columns)

The images are segmented into images of equal pixel size, determined by the number of rows and columns specified by the end user. However, as images may not have a fully divisible number of pixels relative to the specified segmentation parameters, any remaining pixels are allocated to the final row or column of the segmented images, depending on their origin.

7.2.5 Region Evaluation

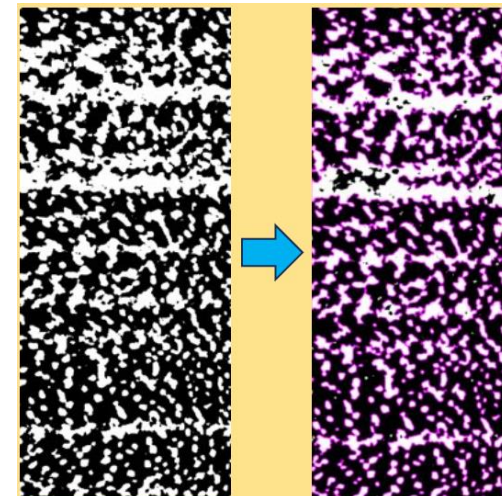


Figure 7.2-9: Image Evaluation Process.

The region evaluation algorithm utilises the images generated from preceding algorithms. Drawing insights from the structural analysis results of the wood veneer, a method for highlighting and examining the white speckles within the wood veneer surface was devised. This algorithm processes the information based on the detected white speckles to generate evaluation scores. These scores are then used to rank the regions, with the results of the evaluation exported to the specified output folder. Figure 6.2.5-1 illustrates the image evaluation process, where the processed image on the right showcases white speckles highlighted by pink contours.

7.2.5.1 Evaluation Scoring

The evaluation scoring was devised utilising the number, variation, and area distribution of white speckles, while closely adhering to the structural analysis results. The scoring method is encapsulated in Eqn. 7.2.5.1:

$$Score = \frac{a}{n} + bR_N + c\bar{A}_N + dR_{max,N} + eR_{min,N} + fV_N + gS_N \quad \text{Eqn. 7.2.5.1}$$

In this equation, a , b , c , d , e , f and g represent weights assigned to respective terms. The subscript N denotes normalization. The terms in the equation are defined as follows:

- n represents the count of white speckles, favouring images with a higher number of speckles.
- R_N measures the ratio between the maximum and minimum sizes of the white speckles, a larger value indicates a wider spread between the sizes, with larger speckles dominating the surface.
- \bar{A}_N signifies the average size of the white speckles, with a higher value indicating a dominance of larger speckles.
- $R_{max,N}$ and $R_{min,N}$ measure the ratio of the maximum and minimum areas of the white speckles to the total wood veneer area, respectively, accounting for individual consideration of the largest and smallest speckles.
- V_N represents the variability in sizes of the white speckles, indicating greater variability with higher values.
- S_N measures the asymmetry of the distribution of speckle areas, with larger values indicating dominance of larger speckles.

The scoring is again normalised within the range $[0, 1]$, where 0 denotes the best region and 1 the worst. This normalization facilitates straightforward comparison between different regions within a group of image datasets and is displayed in the results text file.

Each term in the scoring equation provides valuable insights into different aspects of the distribution and variation of the white speckles on the wood veneer surface. By assigning appropriate weights to these terms, the scoring method effectively ranks the regions of wood veneer from strongest to weakest.

7.2.5.2 Evaluation Result Visualisation

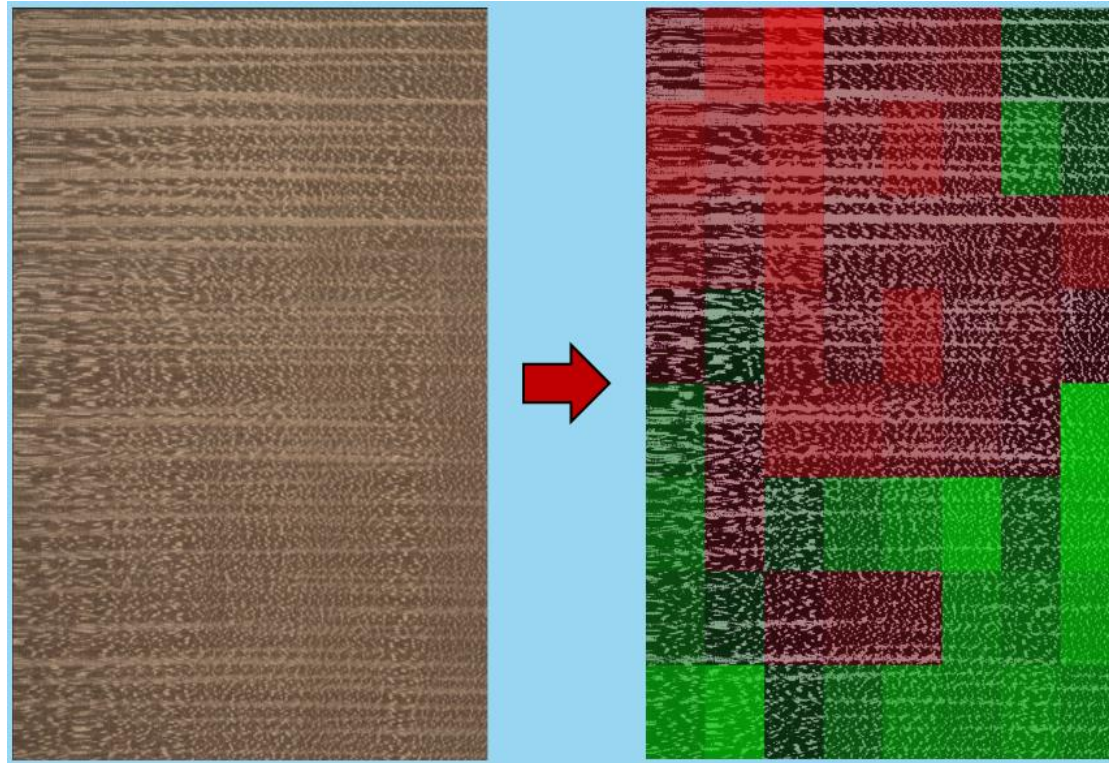


Figure 7.2-10: Region Ranking Visualisation.

To facilitate user analysis, a straightforward visualisation method was implemented to illustrate the evaluation results. This visualisation entails restitched evaluated regions with overlays reflecting pre-normalized scores, with a threshold set as indicated in Figure 6.2.5.2-1 to be 1. Regions are colour-coded from green (strongest) to red (weakest) as defined by the 0° bending structure analysis tests, with scores equal to or below the threshold shown in green, and scores above the threshold in red. Furthermore, the transparency of the overlay adjusts to highlight weaker regions in green and red, aiding users in identifying areas to avoid during manufacturing. This user-friendly visualisation addresses stakeholder concerns by providing clarity and objectivity, thereby reducing reliance on experience-based evaluation.

Ranked based on Scoring!										
Filename	Number of White Polygons	Total Pixel Area	Total Physical Area (mm ²)	Min Physical Area (mm ²)	Max Physical Area (mm ²)	Variance	Skewness	Scoring		
IMG_0004_2_Row5_Col18.png	218.0	349547.0	24470	0.38502	191.53	893.31	2.5301	0		
IMG_0004_2_Row1_Col18.png	236.0	349547.0	24470	0.38502	196.78	698.01	2.9647	0.010731		
IMG_0004_2_Row6_Col16.png	200.0	345113.0	24159	0.38502	246.17	1462.6	3.0466	0.021372		
IMG_0004_2_Row8_Col12.png	192.0	345104.0	24159	0.38502	326.96	2880.9	2.7137	0.023472		
IMG_0004_2_Row7_Col8.png	238.0	349547.0	24470	0.42003	220.48	723.98	3.455	0.036654		
IMG_0004_2_Row8_Col11.png	147.0	345111.0	24159	0.38502	389.96	3424.8	3.6697	0.055459		
IMG_0004_2_Row8_Col17.png	172.0	345113.0	24159	0.42003	440.22	4407.5	3.3499	0.064155		
IMG_0004_2_Row8_Col15.png	193.0	345113.0	24159	0.38502	458.53	4447.4	4.1624	0.074323		
IMG_0004_2_Row8_Col18.png	239.0	349547.0	24470	0.42003	372.63	2338.3	4.644	0.083163		
IMG_0004_2_Row6_Col15.png	142.0	345113.0	24159	0.45503	535.46	6791.5	3.2354	0.085146		
IMG_0004_2_Row6_Col16.png	230.0	345113.0	24159	0.42003	431.82	2105.8	4.3918	0.086436		
IMG_0004_2_Row7_Col6.png	163.0	345113.0	24159	0.56003	387.23	3599.9	2.7456	0.089158		
IMG_0004_2_Row7_Col17.png	157.0	345113.0	24159	0.38502	637.49	7285.4	4.6513	0.10904		
IMG_0004_2_Row2_Col17.png	123.0	345113.0	24159	0.38502	824.44	19396	3.6012	0.11046		
IMG_0004_2_Row6_Col11.png	148.0	345113.0	24159	0.38502	880.55	13614	4.3459	0.13242		
IMG_0004_2_Row6_Col14.png	157.0	345113.0	24159	0.38502	751.6	7698.1	5.1556	0.13481		
IMG_0004_2_Row8_Col14.png	213.0	345113.0	24159	0.38502	682.65	5804	5.9465	0.14378		
IMG_0004_2_Row6_Col17.png	151.0	345113.0	24159	0.38502	737.74	5826	5.993	0.15308		
IMG_0004_2_Row7_Col11.png	166.0	345113.0	24159	0.38502	881.33	8066.5	6.2561	0.17686		

Figure 7.2-11: Region Ranking Output Text File

Additionally, the evaluation results will be documented in a text file, which includes details such as ranked regions, scoring variables, and normalized scores. This offers users an alternative numerical perspective to comprehend the evaluation rankings. Furthermore, the pre-stitched evaluated regions will be saved into a subfolder within the designated

output folder, enabling users to investigate the evaluated regions. An example of the text file format is demonstrated in Figure 7.2.5.2-2.

7.2.6 Validation study

A validation study is needed to be performed for the detection algorithm to find the accuracy of the system. This will be done based on a Receiver-Operator-Characteristic curve (ROC), commonly used in medical practice for determining the

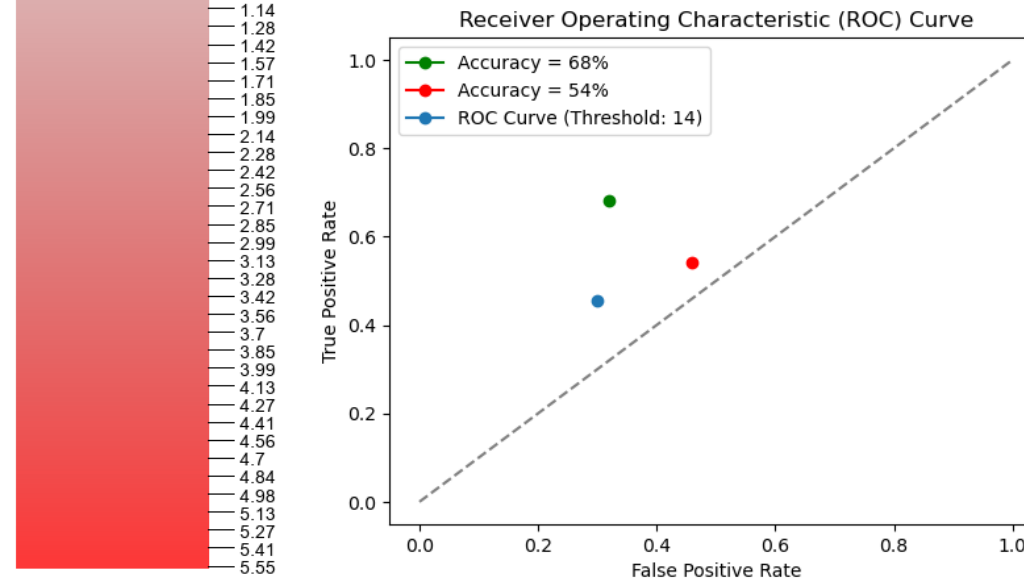


Figure 7.2-12: Left: ROC curve for validation study, right: values for weighting terms in governing equation.

accuracy of a disease test [31]. For a disease test, this method compares the results of a test with the case where the disease was present. This was modified for the purposes of this project to compare a set of samples testing with the cake tier apparatus with the predictions from the code. 50 samples were tested and ranked in order of strength and a threshold of strength was set based on the results, which was then compared to a ranking of the same set of samples produced by the detection algorithm. These were then compared using the matrix below for the number of correct predictions, true positives and negatives, and incorrect predictions, false positives and negatives.

Calculations were then performed to find the sensitivity, probability of a true positive, and the specificity, probability of a true negative. These are plotted on an axis of sensitivity against 1-specificity, which is the rate of false positives. This graph shows how the prediction leans to either true or false predictions, for which the preferred leaning would be towards true for a better confidence in predictions. The first study was conducted using an initial ranking from the code and the results from the test can be seen in **Table 7.2.6-1**. These were used to calculate the accuracy of code from the number of correct predictions against the total predictions, giving an accuracy of 56.41%. This accuracy is far below the aim of this project and therefore the governing equation needed to be optimised to improve its predictions.

Weighting term	Value
ratios_normalized	0.5
avg_areas_normalized	10
normalised_max_area_ratio	1
normalised_var_score	1
normalised_skew_score	0.8
normalised_min_area_ratio	50

Test					
Prediction	Strong	n	Weak	n	Total
Strong	True Positive	a=13	False Positive	c=6	a + c = 19
Weak	False Negative	b=11	True Negative	d=9	b + d = 20
Total	a + b =24		c + d =15		

Table 7.2-3: Initial results with non-optimised code.

Through conducting this study over several iterations, modifying a different weighting in the equation each time, a final accuracy was found with the following results.

Test					
Prediction	Strong	n	Weak	n	Total
Strong	True Positive	a=5	False Positive	c=9	a + c = 14
Weak	False Negative	b=6	True Negative	d=21	b + d = 27
Total	a + b =9		c + d =30		

Table 7.2-4: Results with optimised code

This result, **Table 7.2-6-2**, gave an improved accuracy of 63.41% which is much closer to the aim set for this project, based on the human detection accuracy. This data was also plotted for on the axes of a ROC curve, **Error! Reference source not found.**, which shows the higher true positive rate than false positive highlighting the accuracy. The dotted line represents a 50% accuracy case where there is an equal possibility of a true or false prediction. This accuracy was achieved using the weightings shown in **Error! Reference source not found.** in the governing equation for the detection algorithm.

The ROC plot also includes the point for the initial study, red, and a point that represents the 68% accuracy of human detection, green. These show the amount of the reduced false positives for the optimised code, close to that of the human detection accuracy aim. The reduced true positive compared to the human detection is due to the high score of true negatives for this study which isn't taken into account for the theoretical human detection. The final accuracy obtained for this detection system is therefore 63.41%.

The algorithm has reached a validation accuracy of 63.41%, falling short of our targeted objective. However, it's crucial to note that our accuracy assessment focuses solely on true positives, which inherently carry low uncertainty. In contrast, human evaluations may inadvertently include false positives, leading to greater uncertainty in accuracy evaluations. Consequently, while the detection system consistently achieves approximately 63% accuracy, human assessments may exhibit a wider range of error in detection accuracy.

7.3 Development of System App

The design of the system application represents a pivotal aspect of the project, where various components converge to form a cohesive whole. The system application is required to fulfil the following requirements:

- The process of user input and output analysis is conducted in real-time.
- The software is designed to run on open-source operating systems, which minimises the deployment costs associated with large-scale implementation.
- The user interface is designed to be intuitive and accessible, without the need for complex procedures.
- The software is modular in structure, facilitating separate improvements and maintenance without necessitating a complete system overhaul.

	Web-server based app	Native app
Accessibility	Users can access directly from a browser on any device within the same network	Users must install the app on their device
Environment	Independent of operating system	Dependent on the operating system
Hosting	Hosted on a headless computer or server	Requires hosting with a monitor
Cost	Cost-efficient with faster time to market	More expensive with slower time to market

Table 7.3-1: Comparison of Webserver Based App vs. Native App.

Two different design approaches were considered at the beginning of the development: a web server-based application and a local application. Table 7.3-1: Comparison of Webserver Based App vs. Native App.

provides a comprehensive comparison of various aspects pertinent to stakeholder requirements.

Given the paramount importance of accessibility in adhering to Industry 4.0 automation standards, enabling user access from any device via a headless computer emerges as the optimal solution. This approach offers unparalleled flexibility in plant design and monitoring functionalities, facilitating seamless integration within modern industrial environments.

7.3.1 System Overview

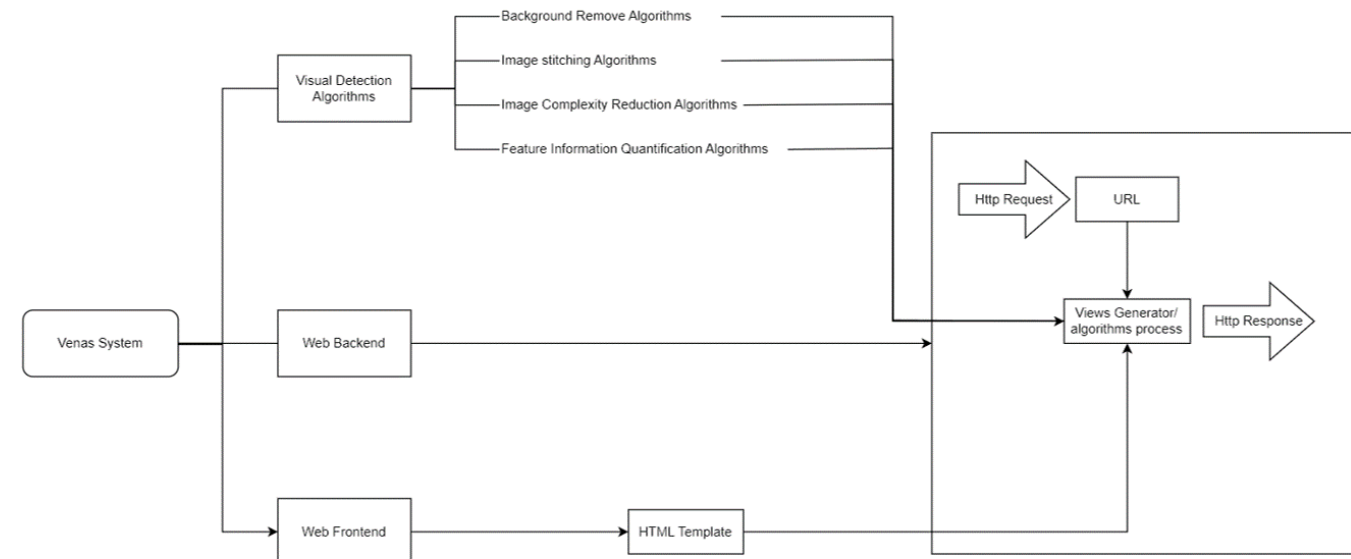


Table 7.3-2: System architecture overview.

Error! Reference source not found. -1 presents an overview of the system architecture, which comprises main principal components. Algorithms are responsible for processing images and identifying problematic wood features. A web frontend serves as a graphical user interface (GUI) for user interaction. A web backend functions as an intermediary and controller between the user and detection algorithms. The system execution sequence is orchestrated by the backend, based on user input, to facilitate seamless interaction.

7.4 Backend Overview

7.4.1 Framework selection

To meet the requirements for cost and power efficiency, a decision was made to utilise a compact and straightforward computer system to drive both the software and hardware components of the system. The Raspberry Pi ecosystem, renowned for its open-source Python support, was selected for this purpose.

	Django	Flask
Usage	Designed for rapid development of web applications	Geared towards straightforward and basic applications
Framework	Follows the Web Server Gateway Interface (WSGI) framework	Offers a lightweight and minimalistic approach
Flexibility	Feature-rich with built-in components for full-stack web development	Provides full flexibility, allowing developers to choose components as needed

Table 7.4-1: Comparison of Django and Flask Frameworks

In consideration of frameworks suitable for the project's needs, Django and Flask emerged as primary contenders within the Python environment. Table 7.4.1-1 provides a comparative analysis of these frameworks. Django, renowned for its feature-rich nature, is a preferable choice due to its ability to streamline system complexity and minimise the need for additional tools. This simplifies maintenance efforts and aligns with the project's design specifications and stakeholder requirements for ease of maintenance.

7.4.2 Folder Processing

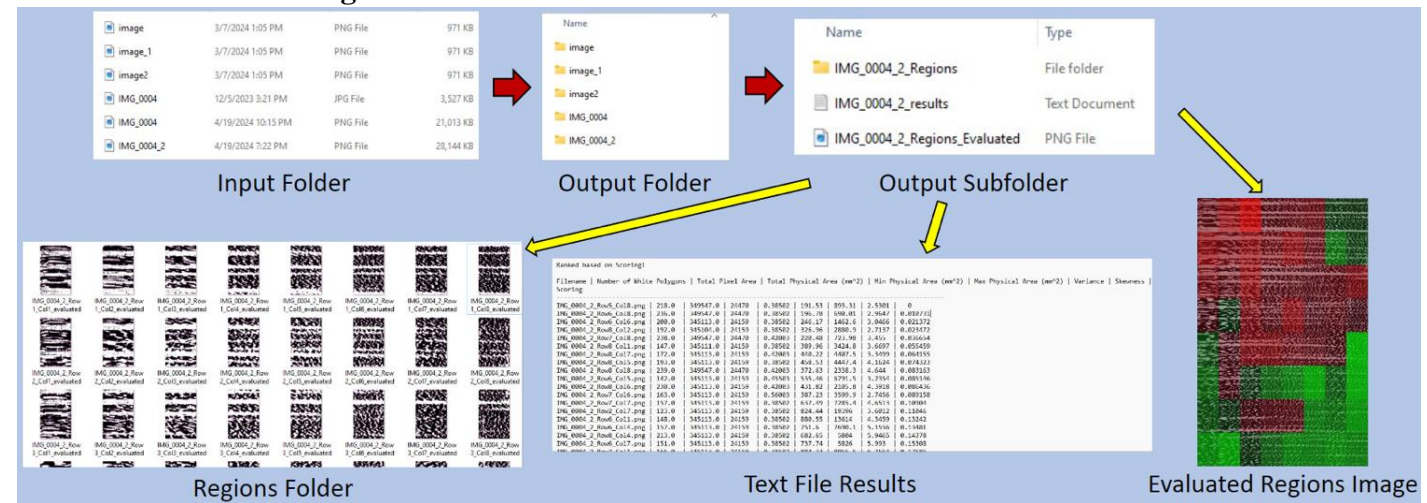


Table 7.4-2: Folder Processing Flowchart

Figure 7.4.2-1 depicts the folder processing system implemented within the backend. Upon capture, images are automatically stored in a predefined input folder, labelled according to the date and time of acquisition. After undergoing the feature detection algorithm, the processed images and associated results are directed to a corresponding subfolder within the designated output directory. This hierarchical arrangement facilitates seamless storage and retrieval of resultant images and analysis outputs, streamlining reference and management processes.

7.5 Frontend Design

7.5.1 CSS framework selection

To achieve a clean and uncluttered user interface. A state-of-the-art, out-of-the-box CSS framework generates the graphical user interface (GUI) layout. The CSS framework includes both CSS and JavaScript-based design templates, allowing users to create responsive designs. Bootstrap and Tailwind are two of the frameworks considered for rapid prototyping of the front end. Table 7.5-1: Comparison of Tailwind CSS and Bootstrap Frameworks. provides a comparative analysis of the two frameworks.

	Tailwind CSS	Bootstrap
Design Approach	Utility-first approach allows for extensive customization	Component-based framework offers pre-designed elements

Customization	Highly customizable, enabling fine-tuning of styles and components	Limited customization options with predefined styles
Flexibility	Provides high creative freedom, allowing for unique designs	Offers less freedom but ensures consistent design across applications
File Size	Tends to result in larger file sizes due to utility classes	Typically results in smaller file sizes due to its modular structure
Community Support	Features a relatively new but active community, growing in popularity	Supported by a large and well-established community with extensive resources

Table 7.5-1: Comparison of Tailwind CSS and Bootstrap Frameworks.

The final design was created using Bootstrap as it provides a consistent design and a smaller file size, which reduces the resource consumption on the computer server and allows more resources to be allocated to other subsystems.

7.5.2 Video streaming method

The GUI design has been carefully tailored to meet the specific needs of operators. To enhance user understanding and operational efficiency, a live stream of the camera view has been seamlessly integrated into the interface. This live feed acts as a real-time feedback reference, enabling operators to make precise adjustments to the positioning of the veneer.

Initially, the video streaming concept relied on the controller periodically requesting images from the camera at fixed intervals. However, this approach proved unworkable as it resulted in lagged video playback and hindered the controller's ability to perform multiple tasks simultaneously. As a result, video streaming would stop whenever other tasks, such as image analysis, were being performed.

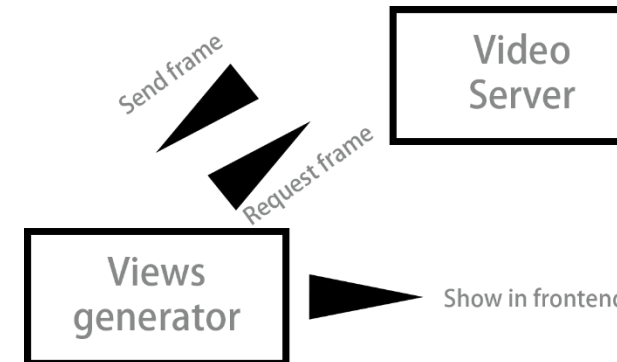
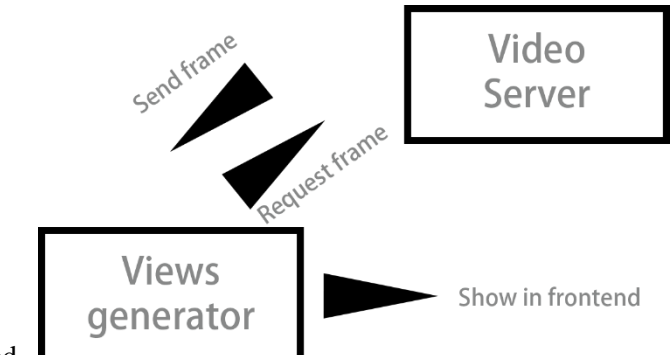


Table 7.5-2: Schematic diagram of the video streaming workflow.



To overcome these challenges, a revised approach was adopted.

Table 7.5-2: Schematic diagram of the video streaming workflow.

shows the workflow of the video streaming method. A web server was created to continuously stream the camera feed, which was then embedded into the user interface. This separation of tasks effectively offloaded the controller, allowing

it to request images from the camera server as needed for wood veneer analysis without interrupting the video streaming process.

7.5.3 Integration with Backend

	jQuery	JavaScript
Development Time	Relatively less due to pre-defined functions	More time-consuming as all code needs to be manually written
Performance	Slower as it requires conversion back into JavaScript for browser execution	Faster as it's directly processed by the browser
Cross-browser Compatibility	Compatible with all browsers out of the box	Code needs to be developed to handle multi-browser compatibility
Size	Lightweight library	Heavier as it constitutes a complete programming language

Table 7.5-3: Comparison between jQuery and JavaScript

To facilitate communication between the front end and the backend, a script is essential for sending messages to the backend for executing specific tasks. Table 7.5.3-1 compares two different methods for enabling this communication. The final design has selected jQuery as the preferred option due to its shorter development time, greater stability, and lightweight nature.

Aims and Objectives Achieved	System Specifications
Data-Driven Approach (Objective 1)	The feature detection algorithm employs a data-driven approach to identify veneer regions to avoid during the forming process.
Output Expectations (Project Scope)	The feature detection algorithm generates a stitched region with overlay for easy visualisation of the evaluation results.
Portability (Objective 3)	The system UI is accessible by any device with a browser.
Environmental Considerations and Power Usage (Design Specification)	The whole system is hosted on a Raspberry PI computer which is a low per consumption device.
User Considerations (Design Specification)	Minimalist and consistent design throughout the UI.
Industry 4.0 (Stakeholder Needs)	The feature detection algorithm is fully automated, requiring just a single click to evaluate each veneer.

Table 7.5-4: Aim and Objectives Completed.

8 Prototyping & Concept Proofing

8.1 Prototyping

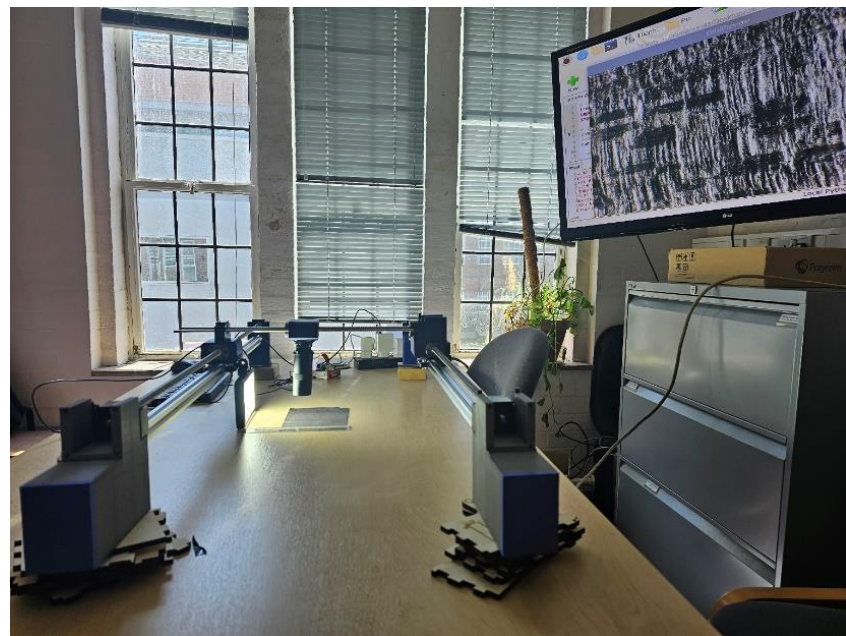


Figure 8.1-1: Prototype of the CMM with working camera module.

Error! Reference source not found. demonstrates the prototype assembly, including the CMM, the camera module, with live preview of the camera displayed on the top left screen. It is tested that the CMM movement are smooth, with the primary axis linear guidance, the v-slot and gantry plate fully functioning in ensuring the linear motion of the movement. The secondary (shorter) axis guidance, which is just 2 simple bars on the side as presented in section 4.3.3, also operating normally as anticipated.

The camera module is connected to a Raspberry Pi 5, also proof to be fully working. Notably, the specification (*Error! Reference source not found.*[25]) of the lens that claims its' object distance from 2.4mm to 36mm is false, with the actual minimum operating distance to be 50mm. Hence, the setup must be raised up, for the camera to focus.

8.2 Investigation of Image Stitching Overlapped Region.

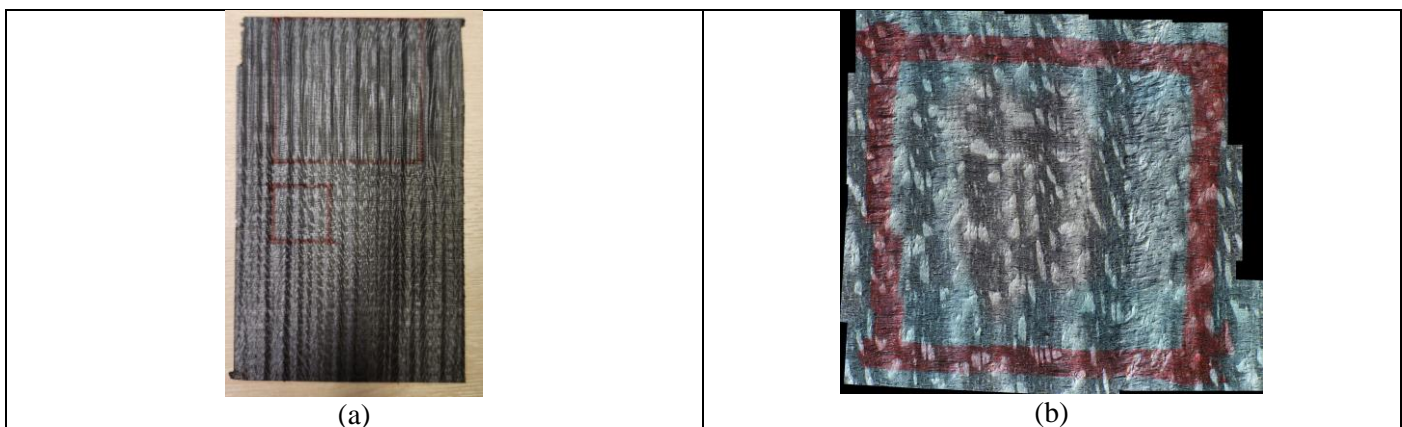


Figure 8.2-2: (a) Showing the veneer sample used for prototype testing, (b) showing the stitched output from the image stitching algorithms.

In order to guarantee the reliability and accuracy of the chosen image stitching algorithms, an investigation was conducted using the prototype setup shown in **Figure 8.2- 1**. **Figure 8.2- 1(a)** shows the sample veneer used for the investigation and **Figure 8.2- 1(b)** shows the final stitched image using the algorithms. This investigation involved determining the optimal overlap region for the algorithms. Through experimentation, it was determined that the optimal overlap region

is 50%. By ensuring that each image has a 50% overlap, the stitching algorithms can accurately recognise features and seamlessly stitch them together with 100% confidence.

9 Summary

9.1 Final Design Proposal

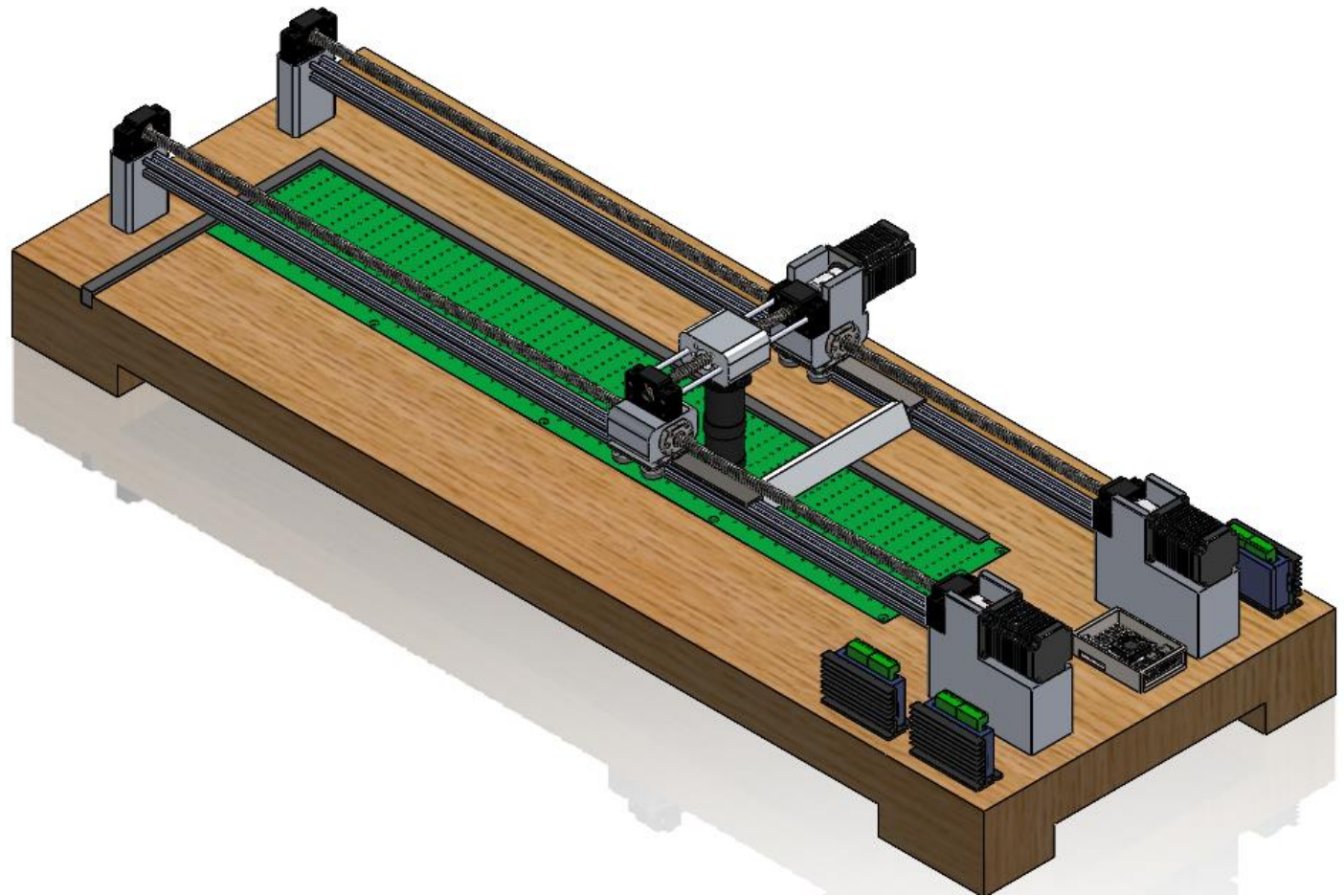


Figure 9.1-1: CAD Design of the Final Design Proposal.

The final design proposal is as shown in **Figure 9.1 - 1**. The veneer is placed on the green plate on the base, aligned using the veneer alignment tool, and condemned by the vacuum system. The camera module, is then transported by the CMM system, capture the pictures of the veneer under the lightning condition provided by the lightning system. Notably, each image of the veneer is designed to be 15.4mm by 11.5mm, hence a total of 62 figures needs to be taken for a 720mm x 125mm size veneer.

Parameters	Target Design Specification	Achieved Specification
Safety	System must be complaint with EN ISO12100:2010. Operating noise of the system < 70 dB	All purchasable components are complaint with EN ISO12100:2010. Operating noise of the system < 35 dB
Environmental Concerns and Material Usage	60% of total components to be	65% of total components are manufactured with

		manufactured with recyclable materials.	recyclable materials. Utilising AA6061 recycled aluminium alloy and Plywood.
Veneer size coverage	720mm x 125mm	950mm x 150mm	
Operating Conditions	System should be fully operational in atmospheric conditions	System is fully operational in atmospheric conditions	
Camera Resolution	12 MP with 1.4 μ m x 1.4 μ m per pixel.	12.3 MP with 1.55 μ m x 1.55 μ m per pixel.	
Camera Zoom	1.7x	0.12x – 1.8x	
Camera MOD	30mm	2.4-36 mm	
Lighting Angle	30-60 °	0-90 °	
Light Intensity	1000 lm	1000 lm	
Light Colour Temperature	5600-6000K	6000 K	
Light Horizontal Distance	7cm to the veneer	7cm to the veneer	
Light Vertical Distance	5cm to the veneer	5cm to the veneer	
Motor Torque	0.54 Nm	1.84 Nm	
Vacuum Pressure Difference	1471.5 Pa	1471.5 Pa with three axial fans.	
Vacuum Plate Background Colour	H : 142°, S : 80-100%, V : 69.8%-80%	H : 142°, S : 100%, V : 69.8%	
Resolution of CMM	0.0189 mm/ $^{\circ}$	Combined Resolution of 0.00771 mm/ $^{\circ}$	

Table 9.1-1: Achieved Specification of Gantry CMM

Parameters	Target Design Specification	Achieved Specification
Portability	Weight: Below 1.4kg for ergonomic portability	Weight of Cake Tier = 0.87kg
Imitate Forming Process	Ability to simulate veneer forming process	Cake tier's bending application imitates forming process
Versatility	Compatibility with various types of veneer	The tool is able to test new veneers and locate stress concentrating features.

Environmental Consideration and Material Usage	Recyclable materials: 60% minimum of apparatus	100% of materials used is recyclable, utilising AA6061 recycled aluminium alloy
User Consideration	Ease of operation without specialised training	Cake tier apparatus consists of a moulding and pressing surface, bend tests can be done via hand.
Varying Diameter	Samples should be able to be tested at varying diameters as different veneers will have a range of critical bending radii.	The apparatus curves have varying diameters from 40mm at the largest tier, based on the calculated critical radii of this veneer, to 15mm at the smallest tie.
Safety	Bend are applied manually using bracket, injuries that are caused by clamping of the two Cake Tier pieces are minor.	

Table 9.1-2. Achieved Specification of Cake Tier Apparatus

9.2 Budget Lists

Budget of Prototyping			
Component Name	Single Price (£)	Amount	Total Price (Shipping and Taxes Included) (£)
Ball Screws (450mm)	27.49	1	126.97
Ball Screws (1000mm)	39.16	2	
V-slots and Gantry Plates	17.28	2	31.09
Adapter Cable for Raspberry Camera Module	3	1	63.99
Raspberry Pi HQ Camera Module	57	1	
Raspberry Pi 5 Power Supply	11.4	1	11.4
Raspberry Pi 5 Active Cooler	4.7	1	4.7
Raspberry Pi 5	79	1	79
Astro Essentials Variable Polariser	34	1	36.95
Pimoroni Microscopy Lens	18.75	1	26.4
Total			380.5

Table 9.2-1: Budget of Prototyping.

Table 9.2-1: Budget of Prototyping. illustrated the budget used in prototyping in **section 8.1** above. The 3D printing service offered by the University is not included in this list, due to the lack of receipt which is not provided. It is evident that the overall budget spend for prototyping does not exceed the constraint of £850, indicating effective budget management.

Sub-System	Final Design Budget List			
	Component Name	Single Price (£)	Amount	Total Price (£)
CMM	Ball Screws (450mm) (SFU1204)	27.49	1	126.97
	Ball Screws (1000mm) (SFU1204)	39.16	2	
	V-slots and Gantry Plates	17.28	2	31.09
	Stepper Motor (23HE30-2804S)	23.28	3	69.84
	Beam Shaft Coupler	3.02	3	9.06

Raspberry Pi and Imaging	Adapter Cable for Raspberry Camera Module	3	1	63.99
	Raspberry Pi HQ Camera Module	57	1	
	Raspberry Pi 5 Power Supply	11.4	1	11.4
	Raspberry Pi 5 Active Cooler	4.7	1	4.7
Lightning System	Raspberry Pi 5	79	1	79
	Pimoroni Microscopy Lens	18.75	1	26.4
Electronics	Ultra LEDs Light Strip	11.28	1	11.28
	WS2815B Light Strip	24.99	1	24.99
	Sunon EE series 80x80x25 Fan	9.66	3	28.98
	TB6600 Stepper Motor Driver	19.2	3	57.6
	Socomec 1A F Cartridge Fuse	0.95	1	0.95
	Cooper Bussmann 5A F Ceramic Cartridge Fuse	0.232	1	0.232
	Cooper Bussmann 3A F Ceramic Cartridge Fuse	0.23	3	0.69
	Voltage Regulator (LM1085)	2.7	1	2.7
	RS Pro DC-DC Convertor	2.98	1	2.98
	Arcolectric (Bulgin) Ltd Illuminated DPST Switch	7.27	1	7.27
	STMicroelectronics 40V 1A Diode	0.328	3	0.984
	Total	561.106		

Table 9.2-2: Final Design Budget List.

proposed the overall budget needed to construct the final design presented is £561.106. Note that the list is based on available product in the market, and those components that can't be bought, as listed in **Table 9.2-3: Components** that are excluded from the Final Design Budget List.

Component	Description
Vacuum Tabletop	Act as base to the design, and also securing the veneer in place. Includes the vacuum chamber and the plate above it with pressure holes.
Vacuum Alignment Tool	Placed on top of the tabletop that helps align the veneer with a 90 degree corner.
Connectors	Components that joint different sub-system together. Includes the components that holds the v-slot and the ball screws, components that connects the two axis in the CMM and the component to hold the camera module,
The light strips platform	The platform to attach the light strips onto. Includes its' connecting component towards the gantry plates.

Table 9.2-3: Components that are excluded from the Final Design Budget List.

10 References

- [1] “Advice for manufacturers - Noise.” Accessed: May 09, 2024. [Online]. Available: <https://www.hse.gov.uk/noise/advice-for-manufacturers.htm>
- [2] A. Lunguleasa, C. Coseceanu, G. Budau, D. Lica, M. G. Matei, and others, “Contributions to the curvature radius and bending capacity of veneers,” *Wood Research*, vol. 59, no. 5, pp. 843–850, 2014.
- [3] H. Yoshihara and A. Itoh, “Influence of large deflection on the measurement of bending properties of veneer by three-point static bending tests,” *Wood and fiber science*, pp. 293–300, 2003.
- [4] R. Duriot *et al.*, “New Perspectives for LVL Manufacturing from Wood of Heterogeneous Quality—Part. 1: Veneer Mechanical Grading Based on Online Local Wood Fiber Orientation Measurement,” *Forests*, vol. 12, no. 9, p. 1264, Sep. 2021, doi: 10.3390/f12091264.
- [5] J. Pyörälä *et al.*, “Assessing log geometry and wood quality in standing timber using terrestrial laser-scanning point clouds,” *Forestry: An International Journal of Forest Research*, vol. 92, no. 2, pp. 177–187, Apr. 2019, doi: 10.1093/forestry/cpy044.
- [6] A. Urbonas, V. Raudonis, R. Maskeliūnas, and R. Damaševičius, “Automated Identification of Wood Veneer Surface Defects Using Faster Region-Based Convolutional Neural Network with Data Augmentation and Transfer Learning,” *Applied Sciences*, vol. 9, no. 22, p. 4898, Nov. 2019, doi: 10.3390/app9224898.
- [7] “How LiDAR Is Becoming an Essential Tool in Forestry.” Accessed: May 09, 2024. [Online]. Available: <https://www.faro.com/en/Resource-Library/Article/LiDAR-Essential-in-Forestry>
- [8] X. Wang, Z. Yu, Y. Zhang, C. Qi, and W. Chang, “Evaluation of ultrasonic-assisted dyeing properties of fast-growing poplar wood treated by reactive dye based on grey system theory analysis,” *Journal of Wood Science*, vol. 64, no. 6, pp. 861–871, Dec. 2018, doi: 10.1007/s10086-018-1768-y.
- [9] Y. Liu *et al.*, “Wood Veneer Dyeing Enhancement by Ultrasonic-assisted Treatment,” *BioResources*, vol. 10, no. 1, pp. 1198–1212, Jan. 2015, doi: 10.15376/biores.10.1.1198-1212.
- [10] “Types of Coordinate Measuring Machine | Eley Metrology,” <https://eleymet.com/>. Accessed: May 09, 2024. [Online]. Available: <https://eleymet.com/2019/03/27/types-of-coordinate-measuring-machine/>
- [11] “CMM: An introduction, types, considerations, applications,” *Wasy Research*. May 2022. Accessed: May 09, 2024. [Online]. Available: <https://www.wasyresearch.com/coordinate-measuring-machine-cmm-an-introduction-types-considerations-and-applications/>
- [12] “What is a Pneumatic Actuator and how do they work?,” *Process Industry Forum*. Accessed: May 09, 2024. [Online]. Available: <https://www.processindustryforum.com/article/what-is-a-pneumatic-actuator>
- [13] mary, “How do ball screws work?,” *How Do Work*. Sep. 2023. Accessed: May 09, 2024. [Online]. Available: <https://howdowork.com/science/physics-mechanics/ball-screws-working/>
- [14] “Belt Efficiency and Energy Saving | TYMA CZ.” Accessed: May 09, 2024. [Online]. Available: [https://www.ty whole="" tma.eu/technical-information/belt-efficiency/](https://www.ty whole=)
- [15] “Rack and Pinion Gear - Working , Design, Application , Advantages.” Oct. 2023. Accessed: May 09, 2024. [Online]. Available: <https://learnmech.com/rack-and-pinion/>
- [16] “Introduction to Lead Screw Selection Selecting a Lead Screw.” Helix Linear Technologies, May 2024. [Online]. Available: <https://9088664.fs1.hubspotusercontent-na1.net/hubfs/9088664>Selecting%20a%20Leadscrew.pdf>
- [17] B. Dengel, “Converting to linear motion using rack and pinion | Gear Solutions Magazine Your Resource to the Gear Industry.” Jul. 2018. Accessed: May 09, 2024. [Online]. Available: <https://gearsolutions.com/departments/tooth-tips/converting-to-linear-motion-using-rack-and-pinion/>
- [18] “10 Steps To Achieve Optimal Ball Screw Selection.” Thomson. [Online]. Available: https://www.thomsonlinear.com/downloads/screws/Thomson_Ball_Screw_Selection_wpen.pdf
- [19] JDS, “Understanding how much power a stepper motor draws,” *Electrical Engineering Stack Exchange*. Jun. 2017. Accessed: May 09, 2024. [Online]. Available: <https://electronics.stackexchange.com/q/313880>
- [20] “Understanding DC Brushless Motor Efficiency & How to Test For It.” Feb. 2024. Accessed: May 09, 2024. [Online]. Available: <https://assunmotor.com/blog/dc-brushless-motor-efficiency/>
- [21] Anon, “PULL OUT TORQUE CURVE OF 23HP22-2804S.”
- [22] C. Ho and M. Mohd Nor, “Tensile behaviour and damage characteristic of recycled aluminium alloys AA6061 undergoing finite strain deformation,” *Proceedings of the Institution of Mechanical Engineers, Part C: Journal of Mechanical Engineering Science*, vol. 235, no. 12, pp. 2276–2284, Jun. 2021, doi: 10.1177/0954406220950349.
- [23] “Simple CNC Vacuum Table,” *Instructables*. Accessed: May 09, 2024. [Online]. Available: <https://www.instructables.com/Simple-CNC-Vacuum-Table/>
- [24] isthatsuperman, “Wanted to try my hand at posters so I made this vacuum table.” [Online]. Available: https://www.reddit.com/r/SCREENPRINTING/comments/f4yjz1/wanted_to_try_my_hand_at_posters_so_i_made_this/
- [25] “100X Industrial Microscope Lens, C/CS-Mount, Compatible With Raspberry Pi HQ Camera | 100X Microscope Lens for Pi.” Accessed: May 09, 2024. [Online]. Available: <https://www.waveshare.com/100x-microscope-lens-for-pi.htm>
- [26] A. Mahram, M. G. Shayesteh, and S. Jafarpour, “Classification of wood surface defects with hybrid usage of statistical and textural features,” in *2012 35th International Conference on Telecommunications and Signal Processing (TSP)*, 2012, pp. 749–752. doi: 10.1109/TSP.2012.6256397.

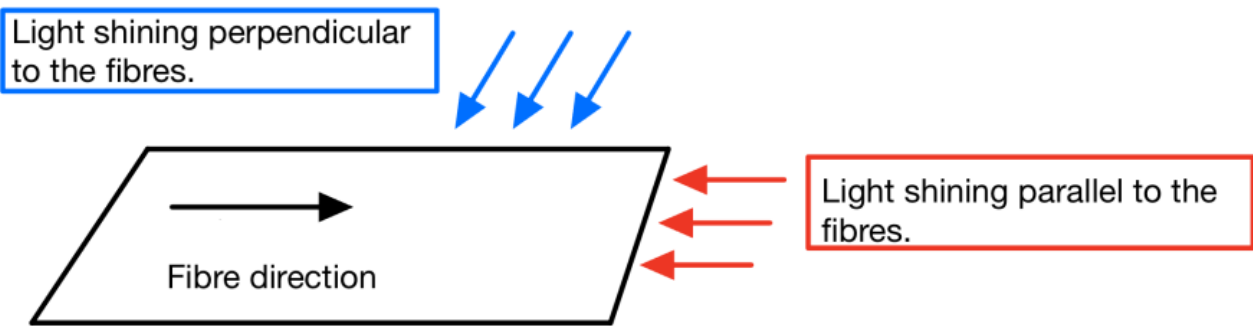
- [27] P. Zhao and C.-K. Wang, “Hardwood Species Classification with Hyperspectral Microscopic Images,” *Journal of Spectroscopy*, vol. 2019, p. 2039453, 2019, doi: 10.1155/2019/2039453.
- [28] P. Wang, E. Fan, and P. Wang, “Comparative analysis of image classification algorithms based on traditional machine learning and deep learning,” *Pattern Recognition Letters*, vol. 141, pp. 61–67, 2021, doi: <https://doi.org/10.1016/j.patrec.2020.07.042>.
- [29] L. Weber and D. Schenk, “Automatische ZusammenfÜhrung zertrennter Konstruktionspläne von Wasserbauwerken,” *Bautechnik*, vol. 99, no. 5, p. 330, 2022.
- [30] N. Otsu, “A Threshold Selection Method from Gray-Level Histograms,” *IEEE Transactions on Systems, Man, and Cybernetics*, vol. 9, no. 1, pp. 62–66, Jan. 1979, doi: 10.1109/TSMC.1979.4310076.
- [31] F. Schoonjans, “ROC curve analysis,” *MedCalc*. Accessed: May 09, 2024. [Online]. Available: <https://www.medcalc.org/manual/roc-curves.php>

11 Appendix A (Section 3: Investigation)

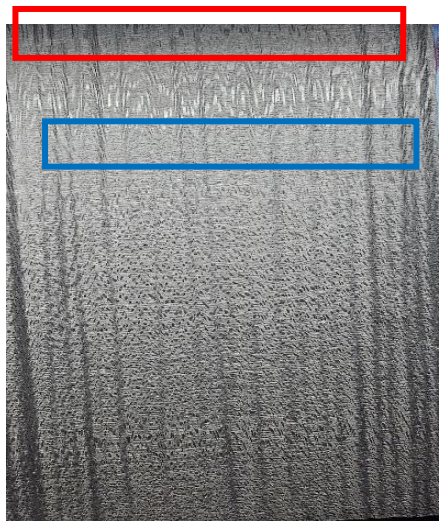
Table 9.2-1: Results recorded for Cake Tie bend tests.

Sample	Tier failed at	Notes on features	Bend application
1	1	Longer vessels	Hand
2	2	Longer vessels, less mismatching of lengths	Hand
3	3	Medium length vessels	Hand
4	2	Medium length vessels	Hand
5	3	Short length vessels	Hand
6	1	medium length vessels	Hand
7	1	Medium and short length vessels	Hand
8	1	Long length vessels	Hand
9	3	Medium length vessels	Hand
10	3	Short length vessels	Hand
11	4	Short length vessels, similar lengths	Bracket
12	1	Longer length vessels, variation in lengths	Bracket
13	1	Longer length vessels, variation in lengths	Bracket
14	1	Medium length vessels, moderate variation in length	Bracket
15	4	Short length vessels, similar lengths	Bracket
16	1	Short and medium length vessels, variation in length close to failure	Bracket
17	1	Short and longer length vessels, variation in lengths	Bracket
18	1	Long and medium length vessels	Bracket
19	1	Long and short fibres, variation in lengths	Bracket
20	2	Short and medium vessels, less variation in lengths	Bracket
21	2	Medium vessels, less variation	Bracket
22	1	Short and medium length vessels	Bracket
23	1	Long length vessels	Bracket
24	1	Long length vessels, less variation in lengths	Bracket

12 Appendix B (Section 4: Hardware)



Appendix B - 1: Orientation of light.



(a)



(b)

Appendix B - 2: : Figure showing light source (a) placed directly above the veneer. (b) 7cm from the veneer.



(a)



(b)

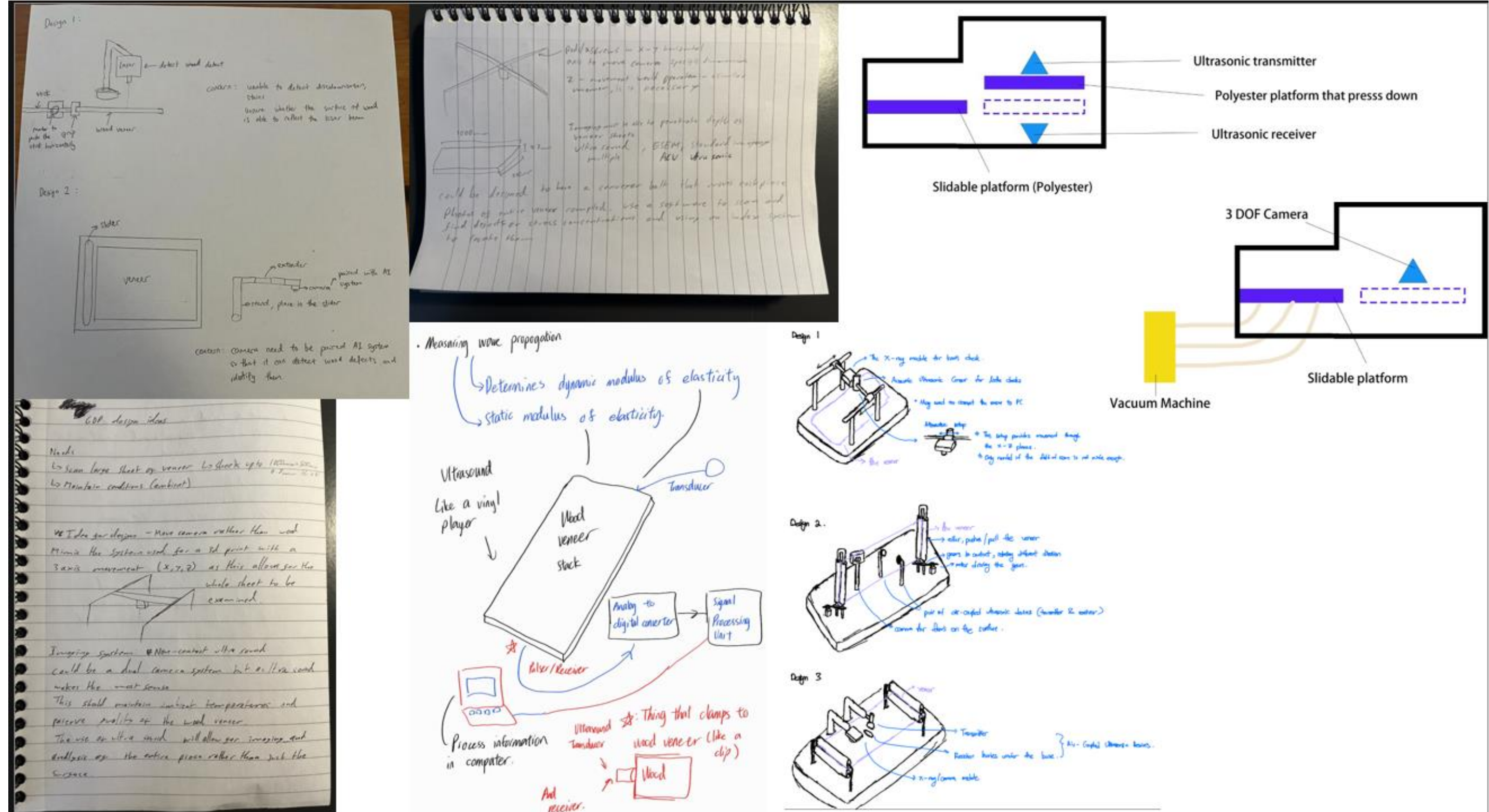


(c)



(d)

Appendix B - 3: : (a) White Diffuser. (b) Red Diffuser. (c) Blue Diffuser. (d) Yellow Diffuser.



Appendix B - 4: Conceptual Designs from the Team